



HAL
open science

Characterizing groundwater flow in a former uranium mine (Bertholène, France): Present status and future considerations

Pierre L'hermite, Valérie Plagnes, Anne Jost, Guillaume Kern, Benoît Reilé, Camille Chautard, Michael Descostes

► To cite this version:

Pierre L'hermite, Valérie Plagnes, Anne Jost, Guillaume Kern, Benoît Reilé, et al.. Characterizing groundwater flow in a former uranium mine (Bertholène, France): Present status and future considerations. *Journal of Hydrology: Regional Studies*, 2022, 44, pp.101221. 10.1016/j.ejrh.2022.101221 . hal-03808838

HAL Id: hal-03808838

<https://hal.science/hal-03808838>

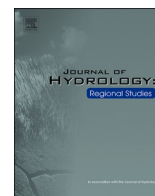
Submitted on 15 Dec 2022

HAL is a multi-disciplinary open access archive for the deposit and dissemination of scientific research documents, whether they are published or not. The documents may come from teaching and research institutions in France or abroad, or from public or private research centers.

L'archive ouverte pluridisciplinaire **HAL**, est destinée au dépôt et à la diffusion de documents scientifiques de niveau recherche, publiés ou non, émanant des établissements d'enseignement et de recherche français ou étrangers, des laboratoires publics ou privés.



Distributed under a Creative Commons Attribution - NonCommercial - NoDerivatives 4.0 International License



Characterizing groundwater flow in a former uranium mine (Bertholène, France): Present status and future considerations

Pierre L'Hermite^{a,*}, Valérie Plagnes^a, Anne Jost^a, Guillaume Kern^b, Benoît Reilé^c, Camille Chautard^d, Michael Descostes^{d,e}

^a Sorbonne Université, CNRS, EPHE, METIS, F-75005 Paris, France

^b AMF, ORANO Mining, 2, route de Lavaugrasse, 87250 Bessines-sur-Gartempe, France

^c Cabinet Reilé, F-25290 Ornans, France

^d ORANO Mining, Environmental R&D Dpt, 125 Avenue de Paris, F-92320 Châtillon, France

^e Centre de Géosciences, MINES ParisTech, PSL University, 35 rue St Honoré, 77300 Fontainebleau, France

ARTICLE INFO

Keywords:

Former mining site
Groundwater flows
Data analysis
Groundwater modeling
Climate change

ABSTRACT

Study region: Bertholène is a former uranium mine in Aveyron, where tailings and waste rocks are stored in a natural valley. This results in acid mine drainage (AMD) at the outlet of the tailings storage facility (TSF), where there is a dedicated water treatment plant.

Study focus: A detailed data analysis was conducted using data from 13 piezometers and from long-term monitoring of the local climate. A 3D model was developed using MODFLOW to understand groundwater flows at the catchment scale and identify flow paths from the contamination sources within the TSF. Previous geochemical modeling of TSFs had indicated that AMD was expected to occur for 50–100 years, therefore the site must be managed with a long-term view. As climate change may affect not only the recharge but also the frequency and intensity of extreme events, its impact on water balance and water levels at the site has to be studied for the next 100 years.

New Hydrological Insights for the Region: Data analysis provides information about the unsaturated conditions within the tailings. Then water balance calculations at the TSF outlet validate the contribution of two different water zones. Modeling using the recharge estimation supports the current functioning of the catchment. The impact study of extreme events shows that the water table should not permanently reach the tailings over the next century.

1. Introduction

From 1948–2001, France mined uranium within its borders. The total production obtained of 76,000 tU over this period represents just a year and half of worldwide production today (WMA, 2020). This activity generated nearly 200 Mt of waste rock and 52 Mt of mill tailings (CartOmines and Orano Mining, 2021). French uranium sites were generally small and exploited either by open-pit mines and/or by underground mine workings.

* Corresponding author.

E-mail addresses: pierre.lhermite@sorbonne-universite.fr (P. L'Hermite), valerie.plagnes@sorbonne-universite.fr (V. Plagnes), anne.jost@sorbonne-universite.fr (A. Jost), guillaume.kern@orano.group (G. Kern), benoit.reile@cabinetreile.fr (B. Reilé), cam.chautard@gmail.com (C. Chautard), michael.descostes@orano.group (M. Descostes).

<https://doi.org/10.1016/j.ejrh.2022.101221>

Received 17 May 2022; Received in revised form 15 September 2022; Accepted 24 September 2022

Available online 28 September 2022

2214-5818/© 2022 The Authors. Published by Elsevier B.V. This is an open access article under the CC BY-NC-ND license (<http://creativecommons.org/licenses/by-nc-nd/4.0/>).

The ore process usually starts by crushing and grinding the ore. Then, depending on the carbonate concentration in the ore, leaching is undertaken with acidic or alkaline substances. Two types of leaching are used depending on the ore concentration: dynamic for high concentrations and static for low concentrations. This process results in a yellow cake from which the uranium is extracted, and also the waste, known as mill tailings. Tailings can be stored at ground level, or underground, or submerged. These facilities contain several million tons of dynamic, static and combined process tailings (BRGM, 1997). Tailings are frequently studied to assist in the prevention of the environmental dispersion of contaminants of concern, and to understand the geochemical mechanisms of the mobility of residual uranium or radium-226, in France and abroad (Déjeant et al., 2014, 2016; Chautard et al., 2017, 2020; Lestini et al., 2019; Ballini et al., 2020; Besançon et al., 2020; Lahrouch et al., 2021; Seigneur et al., 2021). The tailings stored at ground level are usually deposited in piles from 10 m to 150 m high and cover a surface area between one and a dozen hectares. These stockpiles have an environmental impact depending on the type of ore mined, the chemical treatment and the mineral composition (Khoeurin et al., 2019). In France, uranium mill tailings must be stored satisfactorily for the long-term. To achieve this, tailings storage facilities (TSF) are made of several layers acting as a mechanical and radiological barrier. The catchment water is collected and if necessary sent to a treatment plant, with a dedicated environmental monitoring of the water/soil/air/food chain.

When geomaterials enriched in sulfide minerals—mainly pyrite—are in contact with rainfall and oxygen, they react with their environment and can lead to acid mine drainage (AMD, Blowes et al., 2014). AMD is generally characterized by low pH and high concentrations of sulfate, heavy metals (copper (Cu), lead (Pb), zinc (Zn) and cadmium (Cd)) and toxic metalloids (arsenic (As) and selenium (Se)) (Descostes et al., 2004; Tabelin et al., 2018). This is one of the main causes of water contamination worldwide (Bell et al., 2001). In the mining context, this reaction occurs when waste rocks are enriched in sulfide minerals but can be also exacerbated when tailings subjected to acidic treatment have not been neutralized. The long term management of tailings must therefore take AMD into account in order to minimize any damage they may be caused to the environment.

For this purpose, accurate monitoring of the hydrogeochemical variables (water level, discharges, pH, electrical conductivity and environmental tracers) is required to trace and identify potential water contamination (Wolkersdorfer et al., 2020). Data analysis is then used to improve the understanding of the groundwater flows and is essential before any attempt at numerical modeling (Mengistu et al., 2019). 3D-modeling based on the monitoring and analysis of climatic and hydrogeological data also enables the functioning of groundwater flows at the catchment scale, and in particular of the TSF, to be better understood. Numerical models reproducing groundwater and/or surface flows on former mining sites have been used under controlled or real conditions (Aubertin et al., 2002; Mengistu et al., 2015). Many studies have used modeling to simulate either the water rebound after mine closure (Rapantova et al., 2007), the dewatering problem (González-Quirós and Fernández-Álvarez, 2019), the groundwater flow system in an abandoned mine (Tomiya et al., 2020) or to estimate groundwater inflow (Surinaidu et al., 2014). More specifically, one may cite Galván et al. (2016) who modeled the Iberian pyrite belt affected by AMD to optimize remediation efforts in the catchment, and work done by Herr et al. (2007) who developed a catchment-scale AMD model combining hydrological and geochemical data to simulate the mine impact on pH and metal concentration. Different reclamation scenarios, in particular the use of a cover over the tailings, can indeed be tested using a model. Water-cover and/or engineered cover are the main systems used to control AMD generation and reduce radon emanation (IAEA and OECD, 2002). The choice depends on local conditions such as the water budget, climate, tailings properties and storage types (Bussière, 2010; Aubertin et al., 2016; Ethier et al., 2018). Engineered cover systems are used to limit the contact between rainfall water and tailings. In cases where the contamination is assumed to be only short-term, an engineering cover system is not mandatory as long as mining effluents are treated before their release in the environment. The re-vegetation of the surface is in all cases important to control erosion processes (Lersow, 2010) as well as to increase evapotranspiration and thus limit the infiltration of rainwater.

AMD is a long-term process that can occur for more than 100 years and requires sustainable reclamation (Akcil and Koldas, 2006). Yet climate change is likely to alter rainfalls and temperatures over the next 50–100 years. These changes could impact the water table and the surface water discharge at the catchment scale and therefore the geochemical functioning of the TSFs and mining sites (Didovets et al., 2020; Henriksen et al., 2021). Taking into account the impact of climate change on the hydrogeological functioning of these former mining sites will therefore ensure the sustainable management of water and the environment. On the one hand, current studies focus on climate change impacts regarding dam stabilities in mining operations. Tailings dam failures are often caused by intense rainfall events as well as inadequate surface water management (Niekerk and Viljoen, 2005; Hatje et al., 2017). On the other hand, some authors have worked on site reclamation with respect to the performance of tailings cover under climate change, studying its impact on a moisture-retaining layer (Hotton et al., 2020) or showing that a well-designed monolayer cover with an elevated water table should remain effective (Lieber et al. (2022)). But few studies have yet analyzed climate change impacts on water balance and hydrogeological responses in mining areas, even though changes in the frequency and intensity of extreme events due to climate change (Labonté-Raymond et al., 2020) could increase AMD during these events.

In this context, the Bertholène mine represents a model case study in France, which has been studied for a long time (e.g. Ledoux et al., 1993; Schmitt et al., 2002; Triganon, 2013) and is still under long-term environmental monitoring. The Bertholène site is a former uranium mine where mine tailings and waste rocks are stored in a natural valley, incised in the metamorphic basement of the Massif Central. The TSF is located in the middle of the mainly forested Balaures catchment and covers 7 ha out of the 240 ha of the catchment. The stored materials (waste rocks with significant pyrite contents, non-neutralized tailings) in contact with water and oxygen cause AMD, where water with low pH (pH 3.5) and significant concentrations of sulfate concentrations of sulfate (10^{-2} mol/L) and metals $Al = 10^{-4}$ mol/L; $Fe, Mn = 10^{-5}$ mol/L; $U = 10^{-6}$ mol/L) are generated and redirected to a water treatment plant before release into the environment.

At the end of the exploitation in 1995, the site was reclaimed. The hydrogeochemical study concluded that the quality of the effluents from leaching of source terms in the TSF should meet environmental standards without treatment after 50 years (Ledoux et al.,

1993). The choice was therefore made not to cover the TSF and to treat the effluents for this short-term period. Almost 30 years later, even if a significant improvement of the water quality was observed, effluent remains an issue due to AMD generation within the TSF and with acidic water at the TSF outlet. Recent geochemical modeling of the storage facility (Beaucaire, 2021) indicates that AMD is expected to occur for another 50–100 years. This questioned the no cover solution and led the authorities to request additional analyses and the study of alternative solutions from the ORANO Group in charge of the site reclamation. In particular, they called for clarification of the origin of the water at the TSF outlet and better knowledge of saturation conditions in the TSF, as a first step for geochemical modeling. The purpose of this paper is to answer these hydrological questions in order to clarify the current and future hydrogeological functioning of the site, through data analysis and modeling.

This article first presents the analysis of data acquired in the site to better understand the dynamics of the hydrosystem after rainfall events and to clarify the interactions between the waste rocks, the TSF and the water table. Cross-correlations of groundwater level and observed discharges with daily rainfall recorded at the nearby weather station of Rodez were performed. A water balance was calculated using Thornthwaite's approach and based on site observations (rainfall, discharges). A 3D numerical model of the aquifer system of the Balaures catchment was developed based on the recharge calculated from the water balance and the first conclusions of the data analysis. It runs in steady state and saturated conditions representing the average state of the hydrogeological system. The popular and common MODFLOW modeling software (Harbaugh, 2005) has been used in its basic configuration, coupled with GMS visual interface. MODFLOW appears as an international standard to simulate or manage groundwater flows, validated by the authorities, which justifies the choice of this software for the present study. The model helps identify the sub-catchments and test reclamation scenario with a cover over the TSF. The model also allows using particle tracking to identify the preferential flow paths from the potential contamination sources within the catchment. Since the AMD should occur at least during 50 years, the site must also be managed with a long-term view. It is located at the limit between the North and the South of France where the climate change predictions are uncertain regarding the rainfall variation and the modification of extreme events. The impact of climate change on the future hydrological functioning of the catchment was then investigated using daily rainfall and temperature data sourced from the Coupled Model Intercomparison Project (CMIP5) for three climatic scenarios (RCP2.6, RCP4.5 and RCP8.5). The evolution of the water balance as well as the frequency and intensity of extreme events over the next 100 years are evaluated with the CMIP5 simulated data. The study of extreme events observed at the study site complete the analysis to understand the site response to rain events.

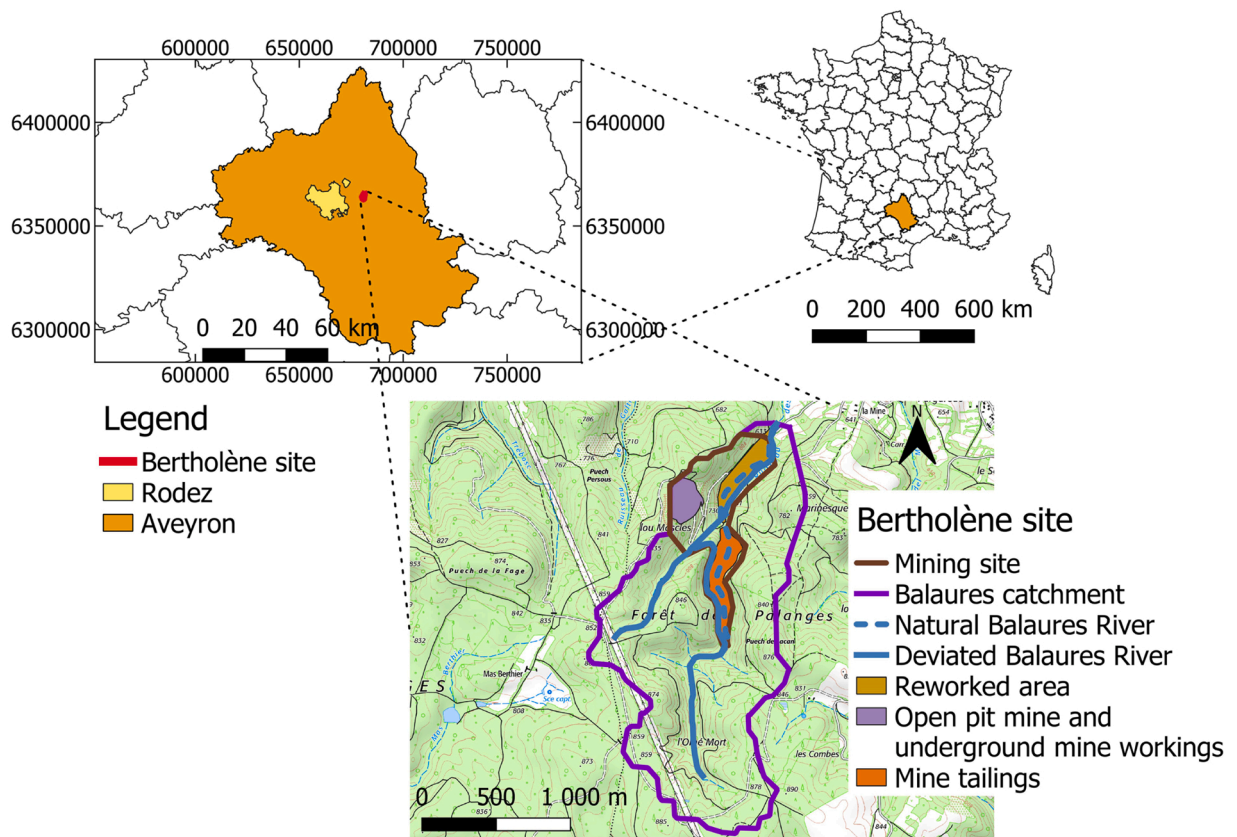


Fig. 1. Location map of the study area (base map from the IGN SCAN25®).

2. Site description

2.1. Location, geology, hydrogeology and climate

The Bertholène mining site is located in the south-west of the Massif Central near Rodez (Fig. 1); it is located in the heart of a 240 ha catchment. The site is surrounded by the Palanges Forest, ranging in elevation from 600 m to 900 m above sea level (m.a.s.l.) with some steep slopes. The catchment is crossed by the Balaures River from south to north. A continuous aquifer is present in the fractured gneiss basement, separated from the Stephanian coal sandstones by the presence of a major ESE-WNW fault (Fig. 2). Further north, the Palanges Fault marks the separation from the Jurassic limestone (Schmitt and Tardy, 1986) and it delimits the hydrogeological catchment. The underground flows are mainly oriented towards the north and are drained by the Balaures River. Successive mine reclamations have significantly modified the downstream part of the catchment where an alluvial water table is found at the bottom of the valley.

The local climate is temperate with a mountain climate influence. A large contrast is observed between winter and summer temperatures. The mean daily temperature varies from around 0 °C in winter to more than 20 °C in summer. The mean rainfall in Bertholène between November 2006 and October 2021 was 1083 mm per year. Two periods can be distinguished. From December to May (winter and spring), some large winter rain events may occur but there are few days with snow. From June to November, the period is drier, with possible stormy events.

2.2. The Bertholène mining site

The mining site covers only 42 ha of the 240 ha of the Balaures catchment south of the Palanges fault (Fig. 2). The site is supervised and monitored by the ORANO Group for its remediation, reclamation and water management.

The Bertholène site was modified by the former mining activities. The southern part is a TSF located in the Balaures valley (drawn in orange in Fig. 1). To avoid contact between the river and the tailings, the Balaures River was diverted to the west of the TSF in a concrete canal. Below the storage facility, the ancient river bed was replaced by a pebble drain which is laid over a geotextile membrane. This drain should collect all water infiltrated through the TSF; it also leads this water to a control basin (BC) where it is collected for treatment.

The northern part of the mining site was extensively reworked during operations and reclamation. Originally the mining facilities were built in this area to process the uranium. Today, a treatment station and several collection basins are located in the same area to control and treat water before discharge into the environment; the area is mainly composed of alluvial deposits. In the alluvial plain, the Balaures River was also slightly diverted to a higher elevation to the east of the site in order to facilitate the development of the mining facilities (leaching stalls, treatment basin and release basin) in the valley (Fig. 1). A non-estimated part of the discharge of the

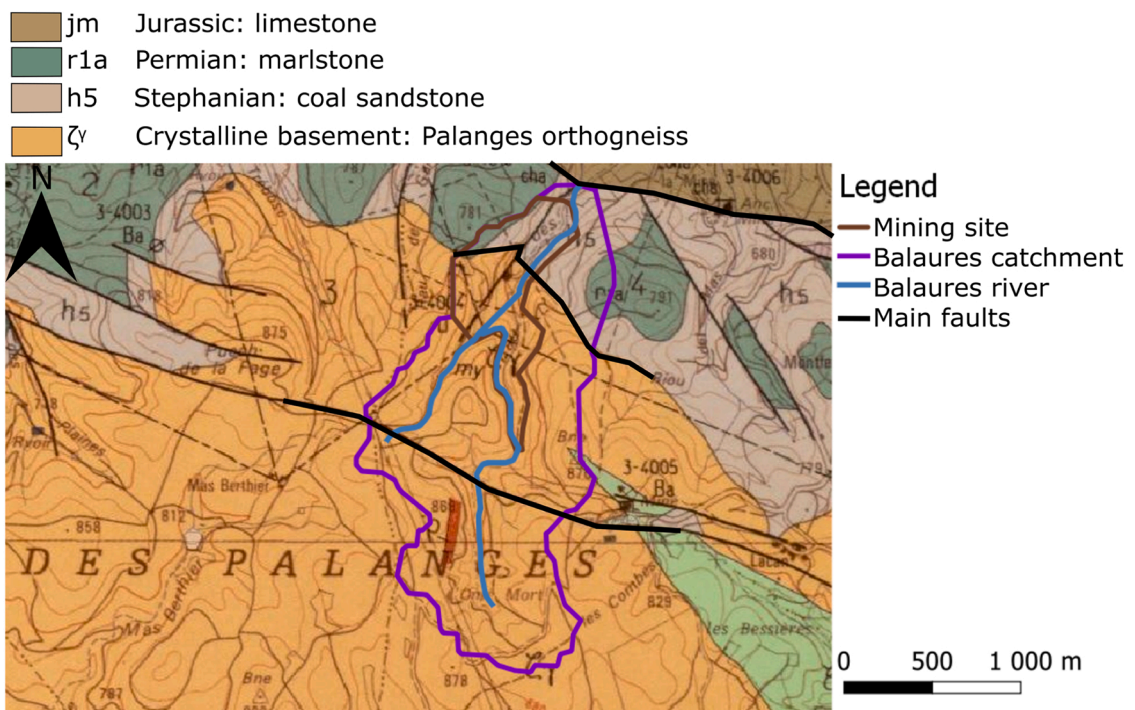


Fig. 2. Geological map and location of the mining site (base map from BRGM, 2020).

deviated river infiltrates into the reworked area and goes back to its original bed.

Water arriving at the treatment plant is collected from three zones: the tailings mining storage, the open-pit mine and the underground mine working (Fig. 3). The water treatment consists of clarification and lime neutralization through successive basins. After the treatment, water goes to post-treatment basins before a final pH check. Its environmental release into the Balaures River takes place 50 m before the discharge station (Q Venturi), itself located 150 m upstream of the outlet of the catchment.

2.3. Ore mining and tailings storage

Uranium extraction at Bertholène started in 1977 and continued until November 1994 with a total production of 750 tU. The ore was extracted by static leaching with sulfuric acid. The uranium deposit extended over a height of about 300 m, from 490 m to 810 m a.s.l. This deposit was mined with both an open-pit mine and an underground mine working. The underground mine was stopped in 1991 because the vein was exhausted. Then the drift (horizontal opening) was partially backfilled (85 %), the pumping was stopped and the water level rose back to its natural level. The open-pit mine extraction was stopped in 1994. 1,100,000 m³ of materials had been excavated to create the operating facilities and build the TSF dykes. The TSF has a length of 700 m, a width around 100 m and it covers 7 ha (Fig. 1). The TSF follows the slope of the natural valley (7 %) with a depth varying from 10 to 50 m from upstream to downstream (Fig. S1, see supplementary material).

The stored materials are varied and piled up in alternating layers. The TSF is composed of 476,000 tons of 0–8 mm particle size. Combined with waste rocks, this mixture is used as protection from the leaching precipitates. Approximately 33,000 tons of precipitates from the neutralization with lime of the acid effluents, which contain gypsum and metal hydroxides, were added to the TSF and intercalated between tailings layers. A pebble drain laid over a geotextile membrane is located at the bottom of the valley in order to collect the water infiltrating through the storage facility. On top of these layers, 30 cm-thick blocks of waste rock separate the tailings from the surface (Fig. 7). At the surface of the storage facility, water sludge resulting from the water treatment since the site closure is stored in storage tanks.

The TSF is now covered with a natural and sparse coniferous vegetation such as pines and small bushes. It is exposed to rainfall and water percolates through it. Water reacts with the remaining pyrite in the waste rocks and generates AMD. Water with low pH (3.5), high concentrations of sulfate (SO₄²⁻ = 10⁻² mol/L) and metals (Al = 10⁻⁴ mol/L; Fe, Mn = 10⁻⁵ mol/L; U = 10⁻⁶ mol/L) drains into the BC at the outlet of the TSF.

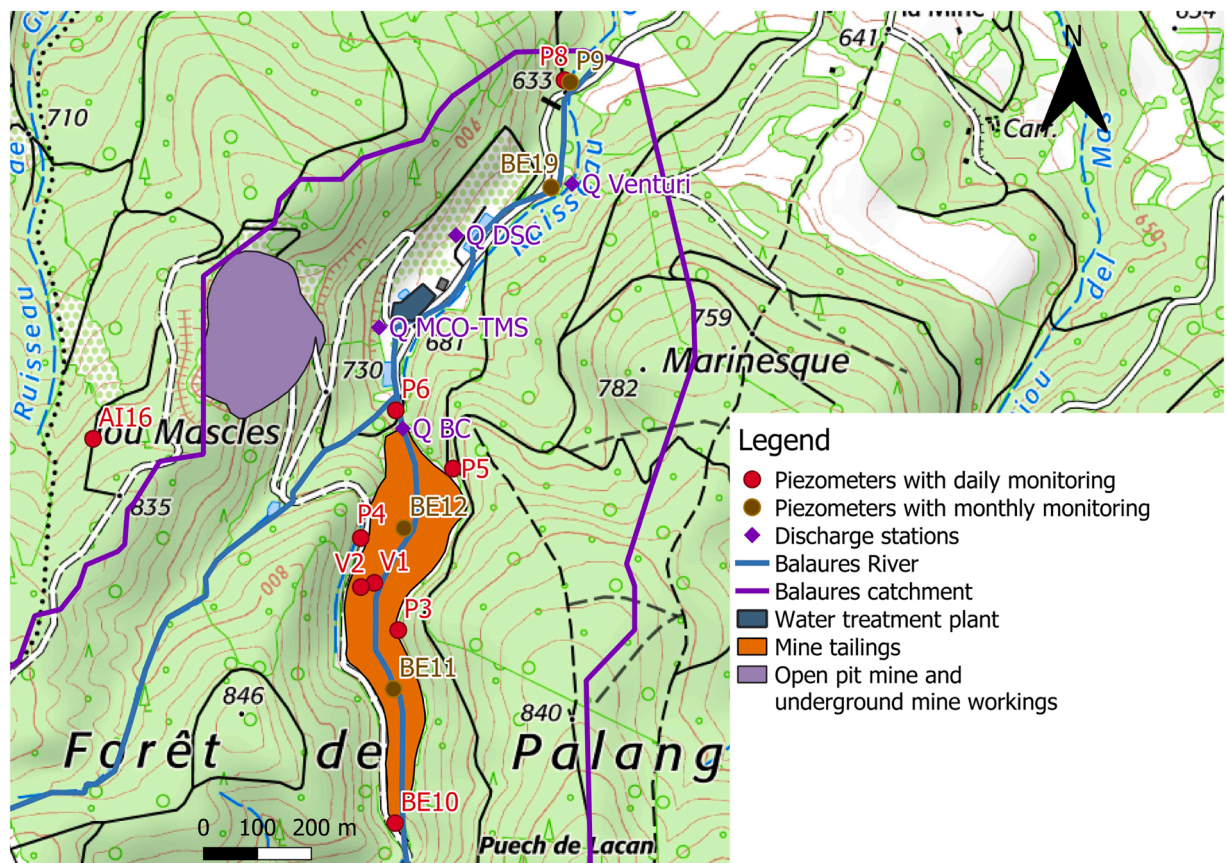


Fig. 3. Location of piezometers and discharge stations in the study area (base map from the IGN SCAN25®).

2.4. Environmental issues

AMD is an issue common to many former mine sites in the world, whose adequate management and long-term remediation initially require a detailed understanding of their hydrological functioning. The methodology developed hereafter to address this issue could therefore be usefully transferred to other former mine sites. In the Bertholène site, the main environmental problem comes from the tailings and waste rocks storage facility with AMD mainly generated by the waste rocks at the storage outlet. It is therefore important in a first stage to quantify the flow conditions within the storage facility for a better understanding of the reaction of the TSF to rainfall. Likewise, the origin of the water arriving at the BC, i.e. at the outlet of the storage sub-catchment, must be explained. These issues must also be viewed through the prism of climate change, which could alter the current water balance. In a second stage geochemical modelling can be coupled to predict the duration of AMD.

3. Materials and methods

3.1. Instrumentation and field measurements

The rainfall data from January 2006 to November 2021 was provided by an in-situ station. These data were originally measured daily and then weekly or monthly since January 2016. To complete the analysis of daily events and catchment reactivity, meteorological data provided by the Météo France station at Rodez have been used to perform daily cross-correlations and extreme-events analysis. It provides daily rainfall and minimum and maximum temperatures for the period 2006–2021. This station is located 25 km away from the Bertholène site at an altitude of 579 m.a.s.l while the mining site is at 700 m.a.s.l. For the period November 2006 to October 2021, the rainfall recorded by Météo France in Rodez (837 mm/year) was 23 % lower than that recorded in Bertholène (1083 mm/year). This difference can be explained by the difference in elevation and topography, the Rodez station being located on a plain while the mining site is in a hilly area.

Records from four discharge stations installed on the catchment are available from January 2006 to November 2021 on a daily then weekly basis (Fig. 3). Three of them measure the water discharge coming from each contaminant zone before it reaches the treatment plant: the open-pit mine (Q MCO-TMS), the TSF at BC (Q BC) and the water originating from the west hillside downstream of the catchment (Q DSC). The last discharge point (Q Venturi) measures the sum of the Balaures River discharges downstream of the catchment and the total discharge from the treatment plant.

Groundwater levels have been monitored on a monthly basis for 23 years (1999–2021), using 13 piezometers, nine of them located inside or around the TSF (Fig. 3). Two new piezometers were drilled in October 2018 in the center of the storage facility (V1 and V2). Most of the piezometers are screened in the most permeable section of the bedrock aquifer (gneiss), however five of them are screened at the interface between the storage facility and the gneiss (BE10, BE11, BE12, V1 and V2). Since June 2018, nine piezometers including the two new piezometers (starting in October) were equipped with SOLINST Levelogger (three) or OTT (six) sensors for a daily monitoring of groundwater level (accuracy for all sensors: ± 0.05 % FS 0–10 m for all the piezometers except for P4 0–20 m).

The electrical conductivity of groundwater has been monitored daily in two piezometers since 2018, V1 in the middle of the TSF and P3 at its eastern edge. This continuous monitoring was supplemented by two sampling missions for all piezometers and outlets. These sampling missions were an opportunity to measure the electrical conductivity at the BC. The high flow sampling mission was in March 2019, at the end of the winter. The groundwater level and the discharges were at their highest, as was rainfall. The low flow sampling mission took place in early October 2019 following a low rainfall summer. Groundwater levels and discharges were low at this time.

3.2. Cross-correlations

Correlation analysis is used in various fields of geoscience, in particular to understand the hydrological functioning of karst systems (Fiorillo and Doglioni, 2010; Larocque et al., 1998). The use of correlation with temporal data can provide information on the response mechanisms of hydrogeological systems (Sahu et al., 2009; Tirogo et al., 2016). Cross-correlation is a comparison between two time series to see if a link exists between the input series x_t and the output series y_t (Eq. (1)); the cross-correlation function r_{xy} is defined by Eq. (2):

$$C_{xy}(k) = \frac{1}{n} \sum_{t=1}^{n-k} (x_t - \bar{x})(y_{t+k} - \bar{y}) \quad (1)$$

$$r_{xy}(k) = \frac{C_{xy}(k)}{\sigma_x \sigma_y} \quad (2)$$

where $C_{xy}(k)$ is the cross-correlogram, n is the time series length, k is the time lag, \bar{x} and \bar{y} are the means of input and output time series, and σ_x and σ_y are the standard deviations of the input and output time series. The time lag corresponding to the maximum value for $r_{xy}(k)$ is the response time of the system to the input signal. The correlation is significant at a 95 % confidence level when $r_{xy}(k)$ is greater than $2/\sqrt{N}$, with N the number of observations.

Cross-correlations were calculated on a daily basis for the period January 2006 to November 2021 with a maximum lag of 40 days, with rainfall as the input signal and discharges at the four stations (Q BC, Q MCO-TMS, Q DSC and Q Venturi) as the output signal; and

for the period June 2018 to November 2021 between rainfall and groundwater level recorded daily by nine piezometers (A116, BE10, P3, P4, P5, P6, P8, V1 and V2). The daily rainfall comes from the Météo France weather station. Using this analysis, the catchment's responses to rainfall events have been studied to understand its reactivity, particularly in the area of the TSF where AMD is generated.

3.3. Water balance

The annual water balance at the site scale is described by Eq. (3) expressed in mm/year:

$$P = AET + R + I = AET + P_{eff} \tag{3}$$

$$P_{eff} = Q = R + I \tag{4}$$

where P is the rainfall, AET the actual evapotranspiration, R the runoff and I the infiltration. For a well-defined hydrological unit, the effective rainfall (P_{eff}) in Eq. (3) should be equal to the discharge Q measured at the catchment outlet (Eq. (4)). AET was estimated using the Thornthwaite method (1948) based on the difference between potential evapotranspiration (PET) and rainfall (P). Two cases are observed (Eq. (5)):

$$\begin{aligned} & \text{if } PET \leq P \rightarrow AET = PET \\ & \text{if } not \left\{ \begin{array}{l} \text{if } P + RU \leq PET \rightarrow AET = P + RU \\ \text{if } P + RU > PET \rightarrow AET = ETP \end{array} \right\} \end{aligned} \tag{5}$$

RU is the soil water capacity fixed at a maximum of 50 mm in this study. RU represents the quantity of water that the soil can absorb and return to plants when PET is higher than rainfall. Eq. (6) describes the PET formula from Oudin et al. (2005) used in this study:

$$\begin{aligned} & \text{if } T + 5 > 0^\circ C \rightarrow PET = \frac{Re}{\gamma\rho} \times \left(\frac{T + 5}{100} \right) \\ & \text{if } not \rightarrow PET = 0 \end{aligned} \tag{6}$$

where Re is the extraterrestrial radiation ($MJ/m^2 \cdot d$) given by the Julian day and the latitude, γ is the latent heat of water vaporization (kJ/kg), ρ is the density of water (kg/m^3) and T is the mean daily temperature ($^\circ C$).

In the Bertholène case, two different hydrological units were considered: the storage facility sub-catchment upstream of the BC (34 ha) and the sub-catchment with Q Venturi as the outlet (230 ha). The discharges for each sub-catchment were respectively measured at Q BC and Q Venturi. The water balances were estimated from monthly data recorded on-site and cumulated by hydrological year for each sub-catchment (November 2006 to October 2021).

3.4. Numerical modeling

A three-dimensional (3D) steady-state groundwater flow model of the catchment aquifer system has been developed using the finite difference code MODFLOW-2005 via the GMS software interface (version 10.4, Aquaveo, 2017). MODFLOW was used with the native packages (recharge (RCH1), well (WEL1)), the solver Preconditioned Conjugate Gradient Solver (PCGS) and the flow package Layer-Property Flow (LPF). Those packages can work with few information about materials properties (horizontal hydraulic conductivity and anisotropy). The saturated flow equation is solved in steady-state conditions with the Preconditioned Conjugate Gradient (PCG) solver with the convergence criteria on head change (HCLOSE) and residual change (RCLOSE) of 0.0001 m and 0.0001 m^3/s .

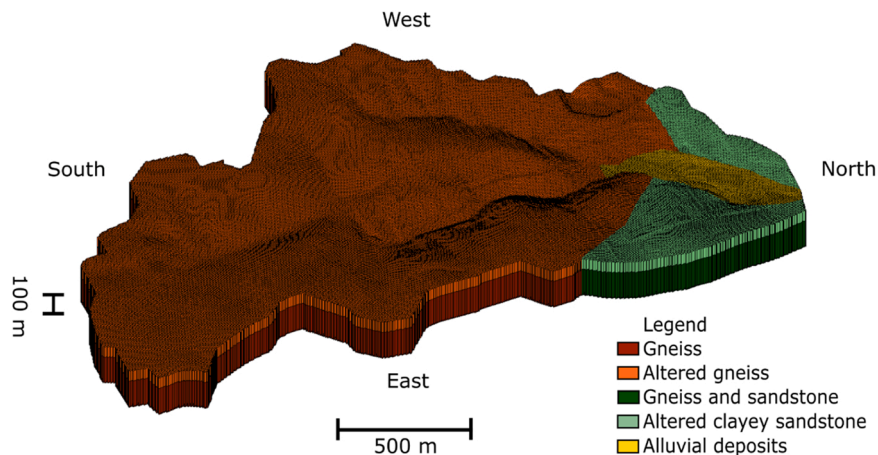


Fig. 4. 3D representation of the simulation domain.

The model is a simplified version of the catchment with only two layers: a 60 m thick unconfined layer corresponding to the weathered bedrock and alluvial deposits, over a 150 m thick confined layer which represents the less permeable deeper bedrock (Fig. 4). The TSF, that overlies gneiss formations over only 3 % of the total model surface, has been removed from the topography and from the model domain due its unsaturated functioning (see Section 4.1). The spatial discretization uses a rectangular grid with 206,385 square meshes with a side length of 5 m that allows for good representation of catchment surface details such as the TSF and the reworked area. The catchment topography is derived from a combination of the French IGN 5 m topographic map (BD ORTHO® 5 m) and a recent 1 m topographic map for the ORANO site specifically created by a land surveyor. The latter represents less than 20 % of the catchment surface. For simplicity and numerical stability, the model of the main local aquifer does not represent the overlying storage facility, and the Balaures River only follows its original course in the natural valley within the TSF section. The topography has been modified to restore the valley to its original appearance prior to the installation of the storage facility, based on the elevation of the old riverbed at the bottom of the valley and by smoothing the sides of the valley.

No-flow boundary conditions were assigned to the lateral boundaries of the domain, which are assumed to align with the catchment divides (Fig. 5). A fixed-head boundary was set for the Balaures River at 0.5 m below the surface in the gneiss, 1 m below the alluvial plain in the northern part, and at 629 m.a.s.l. at the river outlet, a value which corresponds to the mean groundwater level measured close to the catchment output (piezometers P8 and P9). All the small and intermittent creeks were also represented by a constant-head boundary, with a hydraulic head 0.25 m lower than the surface elevation. The main water input of the model is the recharge. The recharge represents the net infiltration estimated with the water balance calculation (506 mm/year = 0.0369 m³/s, see Section 4.3). This recharge is applied to the whole top layer of the model. A second input has been defined because of a small loss (0.00016 m³/s) due to the degradation of the concrete canal, representing 1 % of the canal total flow and less than 0.5 % of the total recharge.

Initial values of hydraulic conductivities (Table 1) were estimated from slug tests from a previous hydrogeological survey of the site (Géostock, 1993) and are assumed homogeneous within each unit except the weathered gneiss. The studied aquifer can be consider a hard-rock aquifer, known to have an anisotropy of hydraulic conductivities (Dewandel et al., 2006). In such aquifers, the horizontal hydraulic conductivity can reach 2–30 times the vertical hydraulic conductivity (Maréchal et al., 2004). A vertical anisotropy of 1/3 is used in the model, which is at the lower end of the range. The model was calibrated starting from these *a priori* values (Table 1) and using the average water level of all piezometers during the period 2006–2021 and the average of the measured discharge at the storage

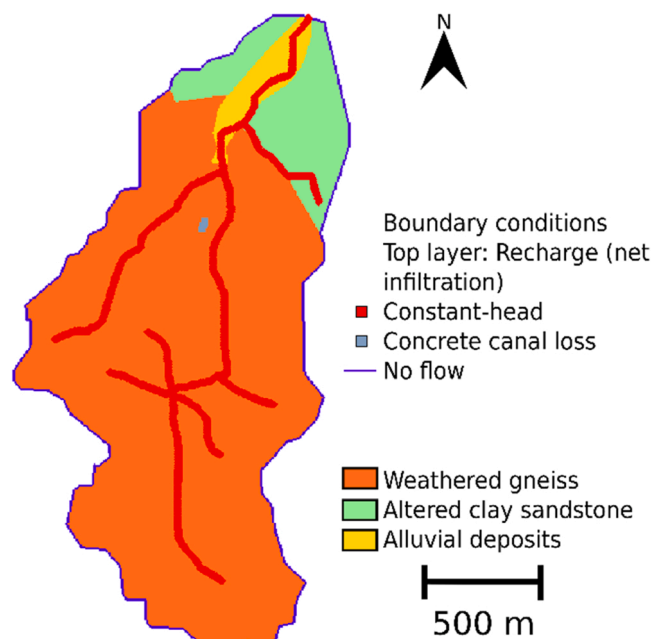


Fig. 5. Boundary conditions of the model and material distribution in the first layer.

Table 1

A priori horizontal hydraulic conductivities from Géostock (1993) and calibrated horizontal hydraulic conductivities from the model.

Layers	Geological horizons	A priori horizontal hydraulic conductivity (m/s)	Calibrated horizontal hydraulic conductivity (m/s)
Layer 1: surface	Weathered gneiss	3.25·10 ⁻⁷	1.5·10 ⁻⁷ – 6.5·10 ⁻⁷
	Clayey sandstone	1·10 ⁻⁷	1.5·10 ⁻⁷
	Alluvial deposits	5·10 ⁻⁵	1·10 ⁻⁵
Layer 2: base	Gneiss	3·10 ⁻⁹	7·10 ⁻⁹
	Mixture of gneiss and sandstone	5·10 ⁻⁹	1·10 ⁻⁸

(Q BC) and at the catchment (Q Venturi) outlets, for the period 2006–2021. All the water levels are measured within the first layer of the model.

Simulations were evaluated in steady-state using the coefficient of determination (R^2) and the following statistical estimators; the mean error (ME), the absolute mean error (AME) and the root mean square error (RMSE), as described by Eqs. (7), (8) and (9):

$$ME = \frac{1}{n} \sum_{i=1}^n (h_{o,i} - h_{s,i}) \quad (7)$$

$$AME = \frac{1}{n} \sum_{i=1}^n |(h_{o,i} - h_{s,i})| \quad (8)$$

$$RMSE = \left[\frac{1}{n} \sum_{i=1}^n (h_{o,i} - h_{s,i})^2 \right]^{0.5} \quad (9)$$

where h_o is the observed water level, h_s is the simulated water level and n is the number of observation piezometers. The estimator values must be as low as possible and close to zero.

Once the model had been calibrated, particle tracking (the MODPATH package available for MODFLOW) was used to visualize the pathlines according to different starting zones and to delineate the hydrogeological sub-catchments. Only forward tracking was used in this study. The use of this package allows us to validate groundwater sources and to visualize groundwater flow pathlines in each sub-catchment as well as within the alluvial area.

3.5. Climate change

3.5.1. Climate data

To analyze changes in temperature and rainfall until the end of the century, six climate projections from the Coupled Model Intercomparison Project (CMIP5) for three climatic scenarios, computed by several European institutes involved in climate modeling, were used (<http://www.drias-climat.fr/>). In total, 18 simulations were analyzed for the period 2006–2098 from the six regional models (Table 2) with three RCP (Representative Concentration Pathway) scenarios as well as 6 simulations for the historical period 1975–2005. Those 6 simulations are considered as reference simulations but not as real observations.

The daily climate data come from regional climate models around Europe. The data were projected onto an 8 km resolution grid and corrected for skew using the ADAMONT method extended to France and implemented by Météo France (Déqué, 2007; Verfaillie et al., 2017), based on the analysis of observation data. The projections from the closest grid point to the site (~3 km) were analyzed (latitude: 44.36120°; longitude: 2.78843°).

The three following RCPs were selected for the study: the RCP2.6 in line with the Paris Agreement, the RCP4.5 considered a more probable scenario and the RCP8.5, the worst-case scenario, for which CO₂ emissions are the highest (IPCC, 2014). The new pathways from CMIP6, the Shared Socioeconomic Pathways (SSPs) have now integrated socio-economic evolution (gross domestic product, demography, governance, education and technology) and are coupled with climate forcing (RCP). A match can be made between the SSPs (CMIP6) and the RCPs (CMIP5) scenarios: SSP1–2.6 and RCP2.6, SSP2 and RCP4.5 and SSP5–8.5 and RCP8.5. In France, the temperature is expected to rise between 2 °C and 5 °C and the rainfall is also expected to rise by 2–6 % according to the RCP scenarios (Soubeyroux et al., 2020). The projected changes in France are different in the northwestern part of France and the southeastern part. The south region of France could be drier with longer droughts and a pattern modification of rainfall, with more rainfall in winter. The location of the site, in the south of France and close to the Massif Central, may have an additional local impact. Table 3 presents the mean overall variation of the 6 models in the study site. For RCP2.6, the temperature variation is lower than that of France and for RCP4.5 and RCP8.5, the variation is the same. For the rainfall, the overall variation shows a decrease in rainfall for RCP4.5 and RCP8.5 that contrasts with the expected variation at the national scale.

3.5.2. Trends analysis: Mann-Kendall and Sen's slope

The non-parametric Mann-Kendall test is commonly used to detect trends in time series of environmental data. As trends can be affected by the presence of negative or positive autocorrelations (Hamed and Ramachandra Rao, 1998), autocorrelation is first performed to check the randomness and the periodicity of the time series data. If randomness is found or the periodicity is statistically

Table 2
Models used for climate change analysis.

Models	General Circulation Model (GCM)	Regional Climate Models (RCM)
CNRM-CERFACS-CNRM-CM5_CNRM-ALADIN63	CNRM-CM5-LR	ALADIN63
CNRM-CERFACS-CNRM-CM5_KNMI-RACMO22E	CNRM-CM5-LR	RACMO22E
ICHEC-EC-EARTH_KNMI-RACMO22E	EC-EARTH	RACMO22E
ICHEC-EC-EARTH_SMHI-RCA4	EC-EARTH	RCA4
MPI-M-MPI-ESM-LR_CLMcom-CCLM4-8-17	MPI-ESM-LR	CCLM4-8-17
MPI-M-MPI-ESM-LR_MPI-CSC-REMO2009	MPI-ESM-LR	REMO2009

Table 3
Mean overall variation for the 6 models for each RCP scenario for the temperature and the rainfall in the studied site.

Scenario	Temperature	Rainfall
	Overall variation (°C)	Overall variation (%)
RCP2.6	+ 0.5	+ 3
RCP4.5	+ 2	- 1.9
RCP8.5	+ 5	- 4

insignificant, the Mann-Kendall test can be performed without altering the data (Kendall, 1975; Mann, 1945). The non-parametric test developed by Sen (1968) is used to estimate the slope of the Mann-Kendall's trend analysis. It calculates the magnitude of any significant trend detected in the Mann-Kendall test.

The Mann-Kendall test and Sen's slope test were performed on the mean annual rainfall and mean annual temperature data. As water balance will be affected by any change in rainfall and temperature, tests were also performed on annual actual evapotranspiration (AET) and annual effective rainfall estimated from a monthly water balance calculation (see Section 3.3). The water balance calculation was performed with the Thornthwaite method to estimate trends on water balance components between 2006 and 2098, independently of the previous results obtained with this method for the historical period. The average variation of rainfall, temperature and effective rainfall for the six models between the periods 2006–2036 and 2068–2098 has been estimated to assess the impact of climate change on the latter.

3.5.3. Extreme events: frequency and intensity

To go beyond the seasonal and annual scales, the analysis also focuses on extreme events that are likely to become more intense and more frequent with climate change (IPCC, 2021). Extreme events can impact the groundwater level below the TSF and create more AMD. Groundwater level monitoring shows that the peaks of water level are reached during the winter period and on consecutive rainy days. To quantify rainfall intensity, our approach consists of analyzing the increase of the amount of rain which falls over three days using return periods. The return periods are estimated using the generalized extreme values (GEV) distribution function which combines three asymptotic forms of extreme value distributions, Gumbel, Weibull and Fréchet, in a unique form (Fisher and Tippett, 1928). This law is mainly used in hydrology to model extreme events and to estimate their return period from daily rainfalls (Santos et al., 2016; Collet et al., 2017; Gaur et al., 2018) on the basis of one maximum occurrence per year. The intensity of each return period has been estimated by taking the highest 3-day rainfall event per year for the historical period between 1975 and 2005, and using it as a reference for comparison with climate projections. Return levels have also been calculated using rainfall from the 18 climate simulations over the period 2006–2036 and at the end of the century period 2068–2098. Analysis of the frequency of exceeding a rainfall threshold allows us to see if the events concerned will be more frequent at the end of the century. The threshold chosen corresponds to the 10-year return period for the historical period, in this case 87 mm. The number of occurrences above the threshold is analyzed for different 30-year periods (1975–2005, 2006–2036, 2037–2067 and 2068–2098).

4. Results

4.1. Spatio-temporal variation of electrical conductivity and hydraulic head in the TSF

Table 4 shows the groundwater electrical conductivity measured in piezometers V1 and P3 and at the BC during the low flow (October 2019) and high flow (March 2019) sampling campaigns and the mean daily electrical conductivity monitored between June 2018 and November 2021. The electrical conductivity measured at BC in October 2019 is 164 $\mu\text{S}/\text{cm}$ for a very low flow at the sampling point ($Q_{BC} = 0.0016 \text{ m}^3/\text{s}$). In March, the flow was higher ($Q_{BC} = 0.0032 \text{ m}^3/\text{s}$) and the electrical conductivity was also higher (684 $\mu\text{S}/\text{cm}$). The highest electrical conductivity is measured in V1 with values above 2000 $\mu\text{S}/\text{cm}$. It reflects the influence of water infiltrated through the TSF where part of the AMD is generated. The electrical conductivity measured in P3 is very low with an average value of 30 $\mu\text{S}/\text{cm}$, representative of the low mineralization of water in gneiss aquifer. It demonstrates that the water in P3 is not influenced by the storage facility. The variation in electrical conductivity in BC is due to the difference in rainfall between the two campaigns. In winter, the vertical infiltration through the storage facility is more important, bringing more water in BC with a high

Table 4
Electrical conductivity for piezometers V1 and P3 and at BC during the low flow and the high flow sampling missions and the mean daily electrical conductivity for V1 and P3.

Electrical conductivity ($\mu\text{S}/\text{cm}$)	Measured in V1 (below the tailings)	Measured in P3 (gneiss aquifer)	Measured at BC
Sampling mission during the low flow period (7 – 14 October 2019)	2310	53	164
Sampling mission during the high flow period (25 March – 2 April 2019)	2150	60	684
Daily mean (June 2108 – November 2021)	2076	30	–

mineralization.

Fig. 6 shows the changes in daily hydraulic heads measured in piezometers inside and around the TSF (locations shown in Fig. 3) from June 2018 to November 2021. Two types of variation are observed. The hydraulic head in the piezometers V1 and V2 located within the storage area (as well as BE11, BE12 and P6, not shown here) shows annual variations with less than 1 m of amplitude, whereas outside the storage facility, annual variations are greater than 3 m with a strong seasonal pattern (BE10, P3, P4 and P5). Peak levels occur during the winter period (December to May) and the highest peaks are observed after intense rainfall (more than 50 mm for several days). The lowest levels are observed at the end of the dry period (June to November).

Fig. 7 exhibits a transversal cross-section of the TSF with the maximum, mean and minimum hydraulic heads observed from daily measurements between June 2018 and November 2021. It shows that the maximum water level remains below the TSF (red dashes), except at the drain level. The drain located at the base of the storage facility can be fed by water coming both from the vertical infiltration through the unsaturated tailings and by lateral groundwater flows from the gneiss aquifer.

4.2. Catchment reactivity

The recent daily monitoring data allow for a more accurate estimation of response times of the water level to rainfall. Cross-correlations between rainfall and water levels in the nine piezometers, as illustrated in Fig. 8a, show a fast reaction and a pronounced response to rainfall with a time lag of about 5 days for the water level in piezometers BE10, V1 and V2. For the other piezometers, the reaction is less pronounced with a time lag that varies from 5 to 16 days. Maximum cross-correlation coefficients are reached within a 5–8 days delay between the rainfall and the discharge at each discharge station, including at the outlet of the storage catchment (Q BC), where the discharge peak appears 8 days after the rainfall (Fig. 8b).

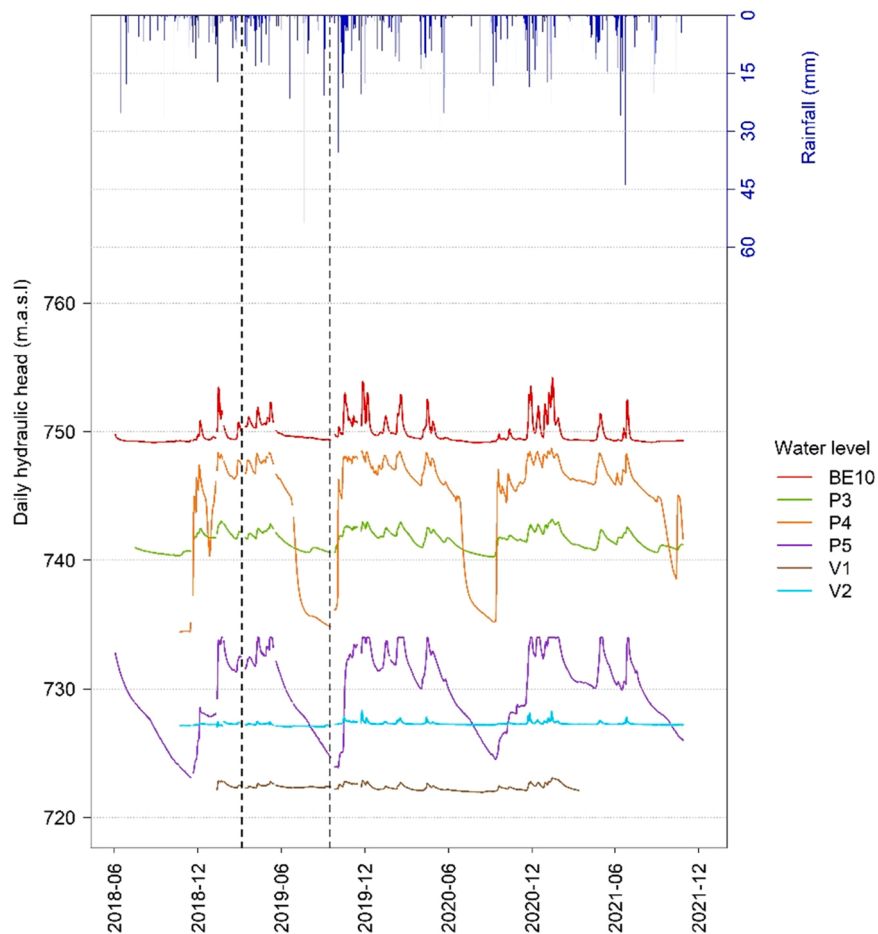


Fig. 6. Observed daily hydraulic heads monitored in the tailings storage facility and daily rainfall at the Rodez meteorological station. The dashed lines correspond to the two sampling missions in March and October 2019.

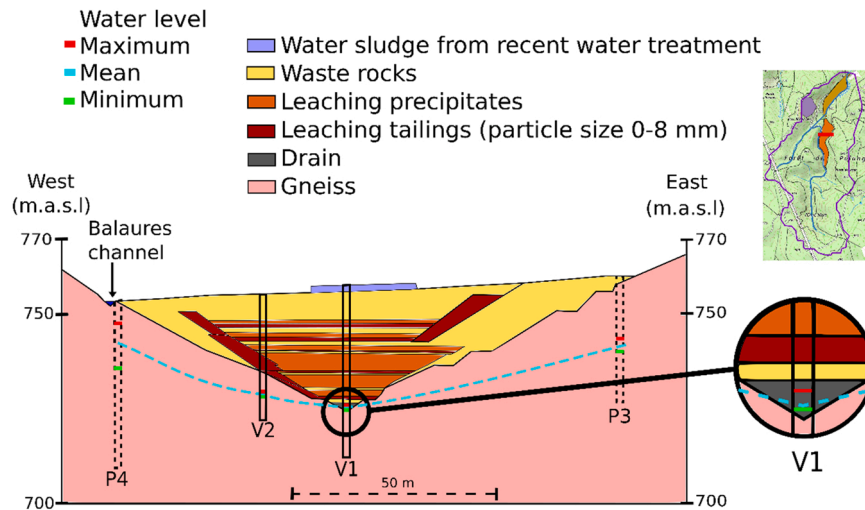


Fig. 7. Piezometric profile across the Balaures valley in the TSF with the mean observed water level in blue. The location of the cross-section is indicated in the insert. P3 and P4 are a projection of these two piezometers because they are not aligned in the same cross section than V1 and V2.

4.3. Recharge estimation

At the mean annual scale, 81.5 % of the discharge at the Q Venturi comes from the Balaures River (Table 5). Of the remaining 18.5 %, which comes from the treatment station, 65 % is from the storage sub-catchment (Q BC), 21 % from the open pit mine drainage area (Q MCO-TMS) and 14 % from the western hill (Q DSC). Q Venturi is the outlet from a hydrological sub-catchment of 230 ha. The zone between the open-pit mine and the western part of the historical facilities is drained to this point by a system of canal and drains. The average annual discharge at Q Venturi is 0.0437 m³/s. Upstream, the storage sub-catchment drains a surface catchment of 34 ha based on the topography of the area. It corresponds to the 7 ha of the tailings storage and an additional surface of 27 ha of forest on the hillsides around the storage facility. The control basin (Q BC) that is supposed to drain this sub-catchment exhibits an average annual discharge of 0.0053 m³/s.

Fig. 9 shows the water balance between November 2006 and October 2021 and the inter-annual average estimated with monthly data aggregated to an annual frequency. The average rainfall is 1083 mm/year. The actual evapotranspiration calculated using the Thornthwaite method is 584 mm/year, which represents 54 % of rainfall. It results in an effective rainfall (P_{eff}) of 611 mm/year, with a small difference (2 %) compared with the mean discharge at the site outlet Q Venturi but 20 % higher than that measured at Q BC, even when considering that the collected water drained by Q BC is a mixture of water coming from the vertical infiltration through the storage (7 ha) and lateral flows coming from the gneiss aquifer (27 ha).

For this catchment which is mainly covered by forest with slopes between 0 % and 7 %, the runoff coefficient can be estimated at a value of 0.17, using the table from the American Society of Civil Engineers (1969). The estimated mean annual runoff is then 104 mm/year and the net infiltration of 506 mm/year is then applied as recharge in the model.

4.4. Groundwater modeling

The calibration of the model at a steady-state condition was performed by varying the hydraulic conductivity of the formations in order to properly reproduce the mean annual piezometric levels in the 13 piezometers of the study area, as well as the discharges observed at the control basin (Q BC) and at the site output (Q Venturi). The calibrated hydraulic conductivities are presented in Table 1.

Fig. 10 shows a good agreement between the observed and the simulated hydraulic heads ($R^2 = 0.993$), to a lesser extent for AI16 which is outside the catchment and BE19 which is in the reworked area. All simulated levels lie within the 95 % confident interval. The ME, AME and RMSE for the calibrated model are - 0.65 m, 3.21 m and 3.78 m respectively. The maximum acceptable value of the calibration criterion depends on the water level magnitude over the domain. The scaled root mean square error (SRMSE), which is RMSE divided by the range of observed water levels, is 3.3 %. It must be less than 10 % to be considered as an acceptable value (Barnett et al., 2012; Mamo et al., 2021). The calibration of the model was thus considered of good quality. The simulated hydraulic heads satisfactorily reproduce the groundwater flow in the gneiss aquifer below the storage area.

The groundwater flow in the southern part of the catchment is drained by the Balaures River and by small creeks on the steepest hills. In the gneiss aquifer (P3, P4 and P5), the flow is oriented directly towards the bottom of the valley. Here the vertical flow across the multiple layers of the TSF corresponds to the prescribed recharge on top of the model. At the storage facility itself, the water table is drained by the ancient bed of the Balaures River (BE11, B12, V1, V2 and P6). Downstream, the groundwater flow is also oriented towards the ancient river bed whereas in the western part of the catchment, where the slopes are steeper, the flow goes straight to the outlet.

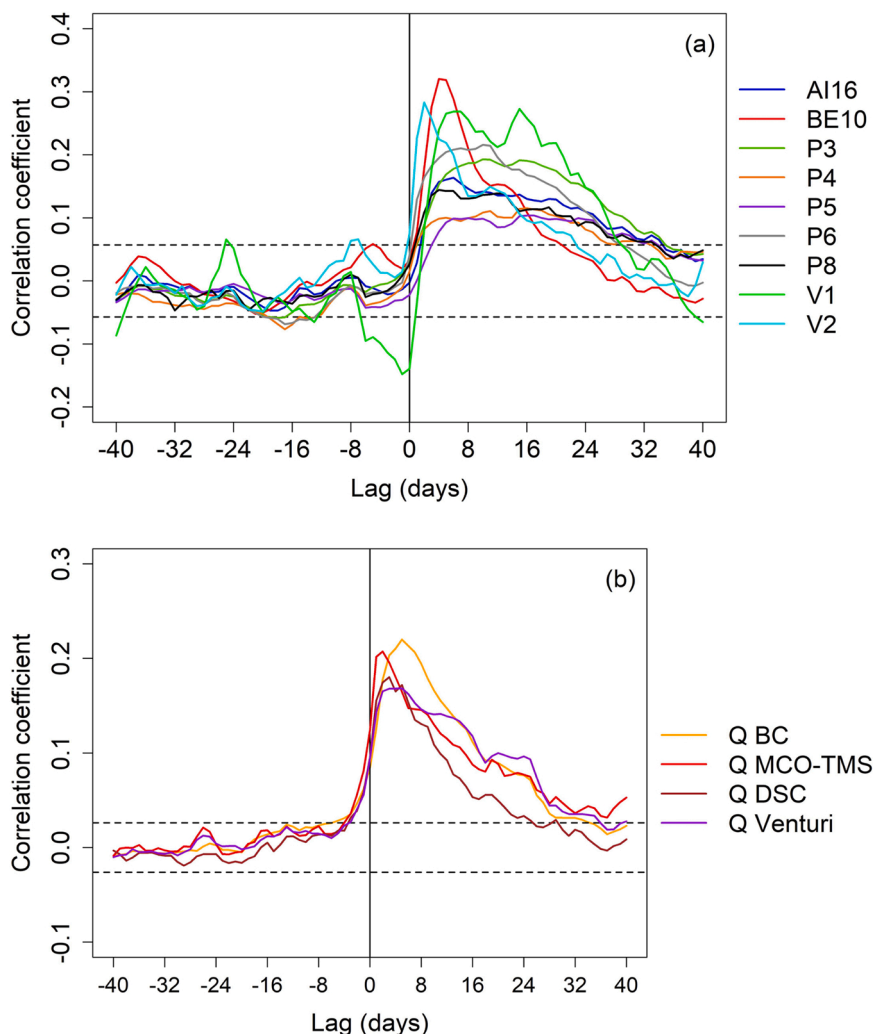


Fig. 8. Cross-correlations at a daily time lag and a truncation at 40 days between (a) rainfall and water levels for the period June 2018 to November 2021, and (b) rainfall and discharges, for the period January 2006 to November 2021. The dashed lines represent the 95 % confidence level.

Table 5

Summary of average annual observed discharges in the site and hydrological surface area for the two catchments of interest. The observed discharges minus the direct runoff are specified as is the simulated discharge by the model. Summary of mean interannual value of water balance variables between November 2006 and October 2021.

Discharge stations	Q BC	Q Venturi	Q MCO-TMS	Q DSC
Average annual observed discharge (in m ³ /s / mm/year)	0.0053 / 490	0.0437 / 599	0.0017	0.0011
Hydrological surface area (ha)	34	230	–	–
Observed discharge minus estimated direct runoff (m ³ /s)	0.0044	0.0363	–	–
Simulated discharge minus estimated direct runoff (m ³ /s)	0.0065	0.0282	–	–

Water balance variables	P	AET	P _{eff}	R	I
2006–2021 mean interannual value (mm/year)	1082.6	584.2	610.6	104	506

If the model gives satisfactory results for hydraulic heads, it does not appear to accurately simulate the observed discharge of the two main sub-catchments of the study area. As shown in Table 5, the simulated discharge at the control basin (Q BC = 0.0065 m³/s) is overestimated by 48 % while the simulated discharge at the outlet of the site (Q Venturi = 0.0282 m³/s) is underestimated by 22 % compared to observations.

Forward particle tracking was used to identify the pathlines of the groundwater flow inside and in the vicinity of the TSF sub-catchment as well as in the alluvial zone downstream of the catchment. For the sub-catchment (Fig. 11), forward particle tracking

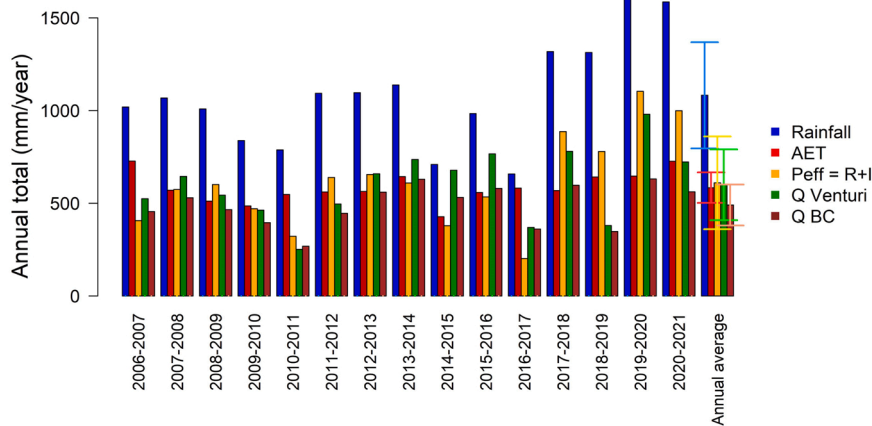


Fig. 9. Water balance for the sub-catchments drained by Q Venturi and Q BC, calculated between November 2006 and October 2021, showing annual average with error bars representing the standard deviation.

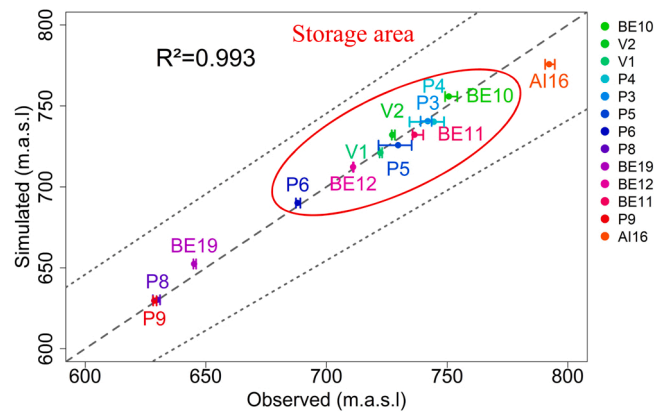


Fig. 10. Scatter plot of simulated vs observed hydraulic heads with minimum and maximum observed values and 95 % confidence interval in dotted lines.

(particles represented by a red circle) was used to delineate the subsurface catchment limits upstream of the control basin. The particle pathlines confirm that the control basin is fed laterally by groundwater flows coming from the hillsides and that the original bed of the Balaures River drains groundwater from the hillsides to the control basin. This subsurface catchment covers a surface area of 40 ha, 6 ha more than the surface catchment previously defined from the topography, whereas a subsurface catchment of smaller size than the surface catchment had been expected to meet the measured flow.

Fig. 12 shows the particle tracking simulation downstream in the alluvial zone. The starting particles are located in layer 1 close to the Balaures surface catchment limits, in order to compare the surface and subsurface catchments and clarify the origin of the difference between the observed and simulated discharges at Q Venturi. It shows that groundwater from the western slopes is not immediately collected by the river but instead flows parallel to the river in the alluvial deposits due to their high hydraulic conductivity and the gentle slopes of the hills. Today, the western part is actually drained by channels and drains and the water flows directly into the Balaures River. If the exchanges between these two areas (+0.0078 m³/s) are added to the previously simulated flow at Q Venturi (0.0282 m³/s), a total simulated discharge of 0.036 m³/s is obtained, equal to the observed one with a slight difference of 0.7 %.

4.5. Climate change

4.5.1. Long-term climatic trends and impact on water balance

In Table 6, according to all scenarios, the mean annual temperature over the next 100 years could statistically increase by 0.5–5 °C at the Bertholène site (mean Sen’s slope: + 0.005 to + 0.052 °C/year). For annual rainfall, no trend is observed for the RCP2.6 scenario. For RCP4.5, only one out of six climate models gives a significant decreasing trend. For the worst-case scenario (RCP8.5), two trends are both significant and decreasing (Table 6).

Concerning the water balance terms at the catchment scale (Table 7), there is no overall trend for AET from the Mann-Kendall test. For the RCP2.6 and RCP4.5 scenarios, annual trends are divergent and mostly not significant, with only three simulations showing a

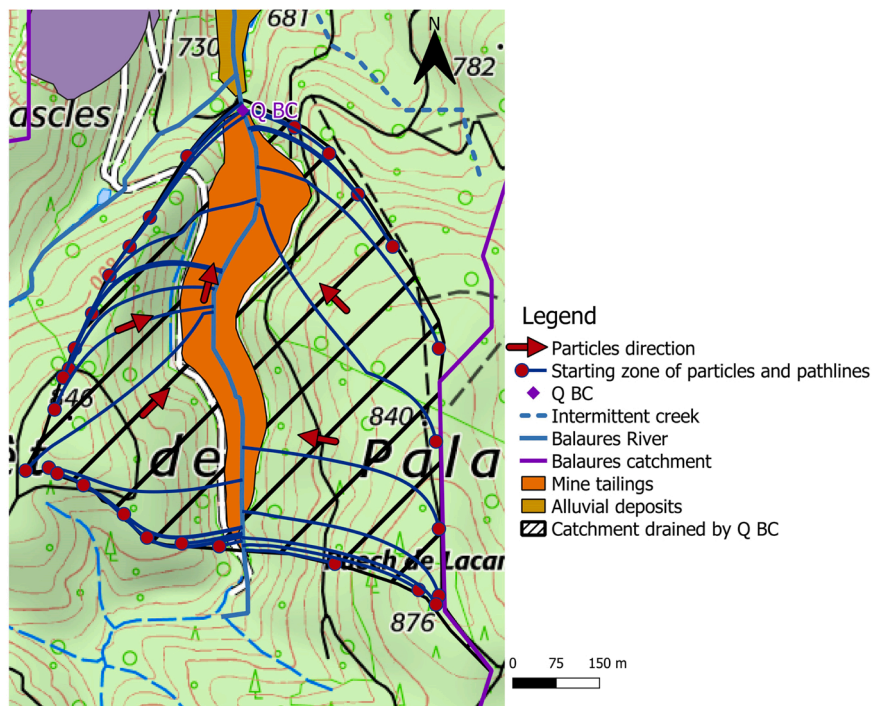


Fig. 11. Particle tracking in the tailings storage area.

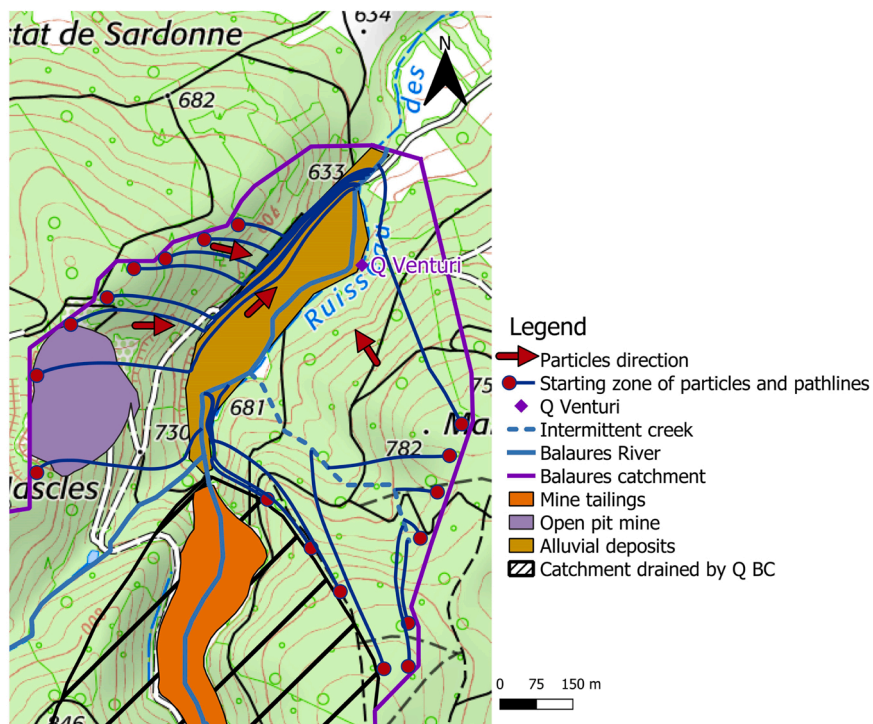


Fig. 12. Particle tracking in the lower part of the catchment.

significant trend. For the RCP8.5 scenario, four out of six trends are significant, half of them showing an increase of AET. Effective rainfall is influenced both by rainfall and AET changes. Only two models out of 18 display a significant trend. Overall the effective rainfall is decreasing for RCP4.5 and RCP8.5 by 2.4 % and 4 %.

Table 6

Summary of the Mann-Kendall tests on temperature and rainfall for the next 100 years with the number of models exhibiting significant trends and the direction of those trends.

Scenario	Temperature		Rainfall	
	Significant trend	Trend	Significant trend	Trend
RCP2.6	3/6	3/3 Increasing	0/6	–
RCP4.5	6/6	6/6 Increasing	1/6	1/1 Decreasing
RCP8.5	6/6	6/6 Increasing	2/6	2/2 Decreasing

Table 7

Summary of the Mann-Kendall tests on AET and effective rainfall with the number of models exhibiting significant trends and the direction of those trends.

Scenario	AET			Effective rainfall		
	Overall variation (%)	Significant trend	Trend	Overall variation (%)	Significant trend	Trend
RCP2.6	+ 3.5	2/6	2/2 Increasing	+ 2.2	1/6	1/1 Decreasing
RCP4.5	– 0.5	1/6	1/1 Decreasing	– 2.4	1/6	1/1 Decreasing
RCP8.5	– 1.2	4/6	2/4 Increasing	– 4	0/6	0/0 Decreasing

4.5.2. Extreme events and their influence on the observed hydraulic head

The impact of extreme events on groundwater level was studied from acquired data on piezometers BE10 and V1 which are the only two piezometers located in the center of the valley. BE10 is located upstream of the storage and V1 is located in the middle of the facility downstream the storage and it is screened at the base of 40 m of precipitates and tailings. The studied events correspond to the maximum water level recorded during the period June 2018 – November 2021. They result from a succession of rainy days between the 19th of January and the 9th of February 2021 for the two piezometers during the wet period.

Fig. 13a shows the water level change in BE10. The peak is reached with a lag of 4 days after 7 rainy days, with a total of 50 mm during the last 3 days. This cumulative rainfall over 3 days corresponds to a 2-year return period event. The water level increased by 2 m in 4 days after a first peak (27 January). The decrease was also rapid right after the rainfall stopped, – 3.5 m in 5 days. This part of the storage facility also exhibits high seasonal piezometric variations (3–4 m) as shown previously in Fig. 6. Fig. 13b shows the water level in piezometer V1 for the same rain event recorded during winter 2021. The highest water level rise is due to consecutive rainy days and the peak is reached after 3 rainy days with a rise of 40 cm. It slowly decreases as the rainfall ceases. During this largest event ever observed during the three years of daily monitoring, the maximum water level observed remained at about 1.5 m below the tailings. The groundwater level also never reached the tailings at the observation piezometers BE11 and BE12 during the 20-year monthly monitoring.

The threshold of the 3-day cumulative event corresponding to the decennial return period is 87 mm over the period 1975–2005. The number of events over this threshold per 30-year period in the 21st century is represented in Fig. 14. For the three periods considered, the number of events should increase from four events between 1975 and 2005 to nearly 8 events, on average, over 30 years. Extreme events should therefore become more frequent during the next century compared with the historical period, while remaining more or less equally frequent over the next 100 years for scenarios RCP2.6 and RCP8.5. For the scenario RCP4.5, there should be an increase from 5.8 in 2006–2036 to 8.3 events at the end of the century.

Fig. 15 shows the estimated intensity of extreme events for several given return periods for the simulated historical rainfall between 1975 and 2005, and for the three RCP scenarios over the period 2006–2036 and the period 2068–2098. For a given return period, the variability of return level is represented according to the six models. The return level is expected to increase by 9–21 % on average at the end of the century for all three scenarios, compared to the historical period. For RCP2.6, events should be more intense for the period 2068–2098 than during the period 2006–2036 by an average of 4.1 %. The same result is observed for RCP4.5 with an average intensity increase of 4.4 % while for RCP8.5, the return levels decrease. For that same scenario, events should be less intense during the period 2068–2098 than during the period 2006–2036 by an average of 4 %.

5. Discussion

5.1. Hydrogeological functioning of the storage area

Thanks to the high frequency monitoring and the presence of two new piezometers within the TSF, the analysis of groundwater level variations demonstrated that the storage facility is in an unsaturated condition with the groundwater level below the TSF. Even for extreme rainfall events with a 2-year return period, the water level still should not reach the tailings base. For the moment, this is the most important rainfall event recorded.

The water collected by the control basin at the storage outlet originates from two sources, as illustrated by electrical conductivities (EC) measured during high and low flow at the drain level in piezometer V1, in the gneiss aquifer in piezometer P3 and at the basin control (Table 4). At the surface, the sub-catchment drained by Q BC is supplied at 80 % from the forest where water feeds the gneiss

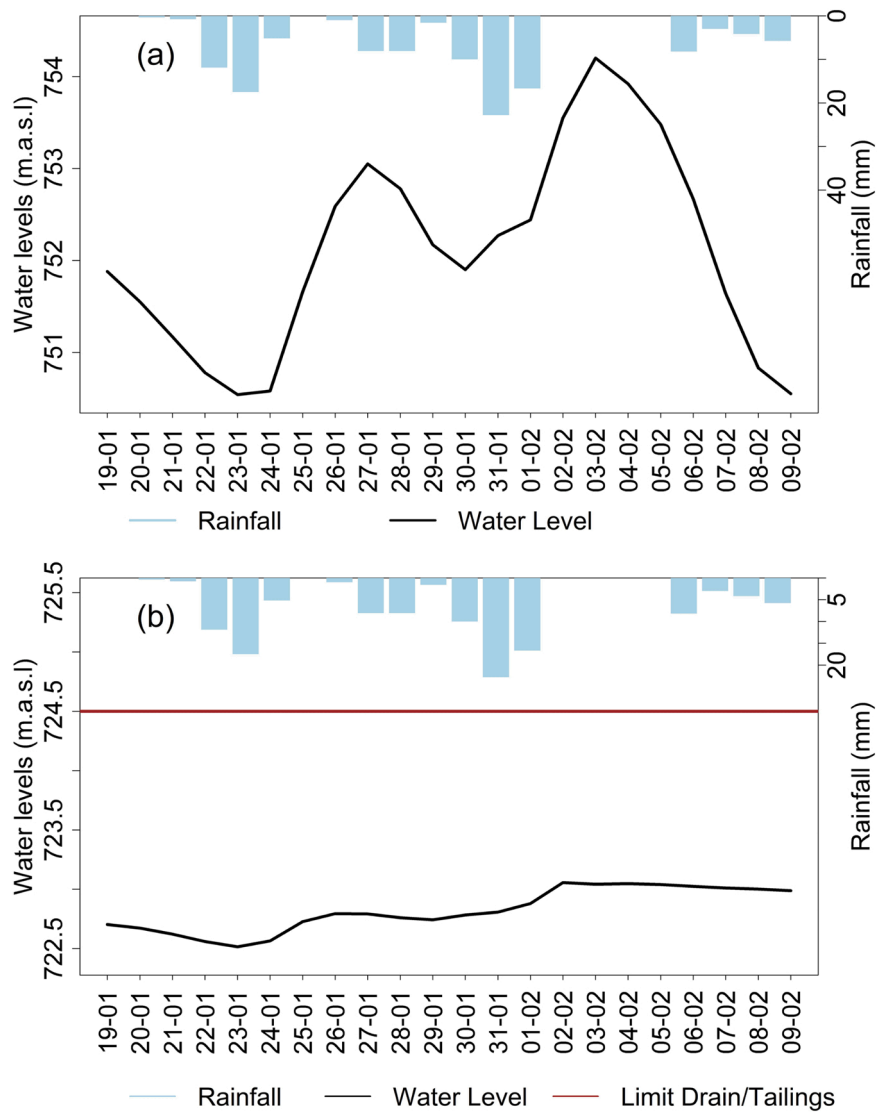


Fig. 13. (a) Observed groundwater level recorded in BE10 piezometer and (b) the highest observed groundwater level recorded in V1 piezometer following the same two-year return period event.

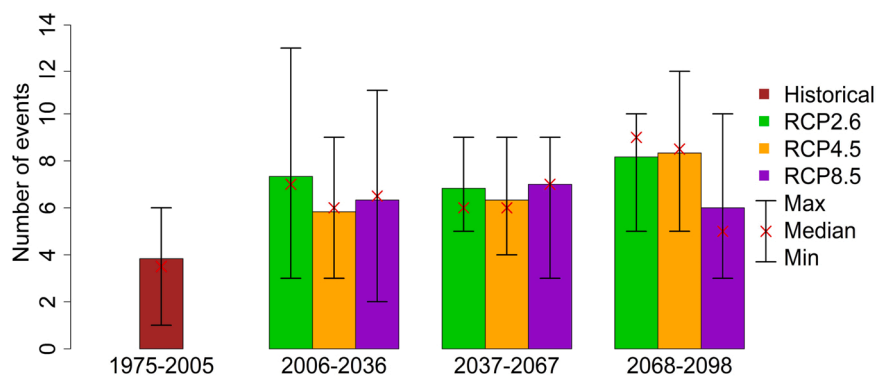


Fig. 14. Mean number of events over the threshold (87 mm, decennial return period) over the six simulated historical period and for the six simulations for each RCP scenario and three successive 30-year periods over the next century with the maximum, minimum and the median.

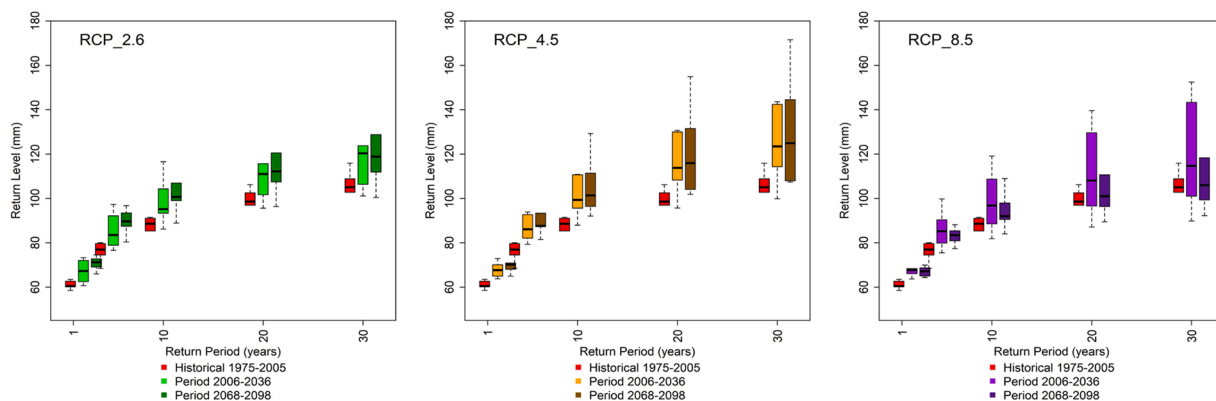


Fig. 15. Estimated return levels for the three RCP scenarios in 2006–2036 and 2068–2098 and the historical period (1975–2005). Return levels are estimated for 2, 5, 10, 20 and 30 years.

aquifer, and at 20 % by the TSF through which water infiltrates vertically. During high flow period, the combination of 70 % of groundwater from the gneiss aquifer and 30 % from the tailings zone gives the measured EC value of 684 $\mu\text{S}/\text{cm}$ at the control basin. During low flow period, the repartition corresponding to the measured EC value (164 $\mu\text{S}/\text{cm}$) is very different, with only 5 % from the tailings zone and 95 % from the hillsides. Water percolation through the tailings is limited during summer by less rainfall and high evapotranspiration, while the bedrock aquifer acts as a reservoir, storing water in winter and releasing it in summer. It is assumed that the drain is continuously fed by vertical infiltration as the electrical conductivity measured in V1 always remains high (Fig. S2, see [supplementary material](#)) indicating the presence of high mineralized water in this piezometer all year long. Vertical infiltration occurs through two mechanisms: continuous Darcy-type flow and non-continuous rapid preferential flow (see [Section 4.3](#)). The second mechanism could be of real importance with climate change and extreme events. [Kalisman et al. \(2022\)](#) showed that pulsed pressure wave flow, which can be likened to sudden water injections or extreme events, generated 75 % more solute mass compared to continuous Darcy-type flow. The AMD generation could then be increased. It is also assumed that the old river bed still acts as a drain for the gneiss aquifer, as illustrated in the numerical model by the convergence of groundwater flows towards the former river bed (here defined as a constant head boundary condition).

5.2. Catchment scale groundwater flow

The annual water balance estimated using the Thornthwaite method, a *PET* calculation based on the Oudin formula and a *RU* of 50 mm maximum is well balanced at Q Venturi. With the estimated recharge (506 mm/year), the measured discharge (minus runoff) at Q Venturi is well reproduced by the model, taking into account the flow drained by the alluvial part on the left bank. There is agreement between the surface and subsurface watersheds at the scale of the Balaures catchment.

With the same calculation, the water balance at Q BC is overestimated by 20 % for a hydrological surface of 34 ha. A sub-catchment area of only 27 ha would be required to balance the water budget at Q BC. However, the model does not confirm this hypothesis, with a subsurface catchment determined using particle tracking reaching as high as 40 ha. The increase in hydraulic conductivity of the deep layer within a reasonable range did not allow the creation of deeper circulations bypassing the drain under the tailings. The hypothesis of lower effective localized rainfall is also not supported by the presence on the TSF of a sparse vegetation cover and coarse materials on the surface that facilitate infiltration. The model was unsuccessful in providing constraints on the value of the recharge, as the simulated heads in the storage area were not sensitive to the imposed recharge value, which we varied between -5% and $+20\%$ of the initial value. Only the *ME* criterion decreases as recharge increases. Therefore, it is possible that the presence of the geotextile membrane at the base of the drain, which is not represented in the model, partially limits drainage from the catchment area to the control basin. In any case, however, it facilitates the recovery of any water that has seeped into the TSF and is then stored in the control basin. Finally, we cannot exclude the possibility that the quality of the flow measurement at the control basin is part of the explanation for the water balance discrepancy. In addition, the potential evapotranspiration calculated for the catchment is 662 mm/year, which represents 61 % of the rainfall. The *PET/P* ratio for the Bertholène site is the same as for other small catchments in the area when using the same Oudin evapotranspiration formula (French Hydro database, [Brigode et al., 2020](#)). In the equivalent catchments (1.2–24 km^2) located around the Bertholène site (O5010535, O5000510, O5445510 and O5055310), this ratio is less than 65 %. We can therefore assume that the Thornthwaite water balance calculation does work at Q Venturi between November 2006 and October 2021 and can be used to estimate the water balance in the context of climate change, considering all other parameters equal, including vegetation.

5.3. Use and limitations of the hydrogeological model

In its native version, MODFLOW cannot simulate unsaturated flow. The UZF package has been developed to meet this need but it is mainly designed to compute the evapotranspiration and the recharge in unsaturated areas. Despite that, MODFLOW has been chosen in

this study. First, the knowledge of the particle size and the parameters to describe the unsaturated medium within the TSF was very imperfect and not sufficient to run adequately the UZF package. Second, the goal was to simulate the average groundwater flow at the catchment scale. The TSF that overlies gneiss formations over only 3 % of the total model surface, was therefore removed from the aquifer system model domain due its unsaturated functioning inferred from the available data (see Section 4.1). In reality, from a hydrogeological point of view, the TSF delays the impact of effective rainfall by 5–16 days into the drain located below the TSF due to the infiltration through the tailings storage (see Section 4.2). As the model runs in steady state conditions and represents an average hydrogeological functioning, this delay is not taken into account at the annual scale.

The use of a variable saturation flow model would certainly have been more appropriate but also much more expensive to implement in 3D and at the catchment scale. A transient model would also have been useful to simulate seasonal variations and determine how groundwater levels and discharges would change during future wet and dry periods (Ethier et al., 2018; An et al., 2022). Simulation of flows taking into account the delay due to the TSF would provide information on flow velocity in summer and winter and on possible preferential flows in the TSF. In addition, the development of a transient model would allow the simulation of the site's fate for the next 100 years. In particular, it would allow for the simulation at the site scale of the groundwater level during extreme events today but also in the future. These events would not have the same impact on groundwater level in dry periods as in wet periods regarding the initial groundwater level conditions (Petpongpan et al., 2021). The observed extreme events (Fig. 13) occurred during the winter period with a high groundwater level. But the reaction of the groundwater level is unknown during the dry period in case of heavy rainfall, dry soil and low groundwater level.

Despite all those simplifications and limitations, the model was used to study the impact of an engineered system cover over the TSF on the hydrogeological functioning of the aquifer system. This cover is expected to limit or stop the infiltration through the TSF in order to reduce AMD generation. To test this scenario, the recharge over the TSF surface (7 ha) was set at 0 mm/year. As the main input in the model is the recharge, the modification of the recharge impacts directly the groundwater level and discharge, mainly at the TSF scale. Compared to the reference model, the average decrease in simulated water level with cover would be about 1.6 m in the TSF area and the decrease of the discharge is 20 % at Q BC and 3 % at Q Venturi. The discharge would still be 0.0052 m³/s at Q BC and mainly composed of water from the gneiss aquifer with an average pH of 5.7, above the environmental release limit (pH = 5.5). The acid mine drainage at the TSF outlet would be slightly reduced because gypsum and pyrite contained in the tailings will be isolated from the rainfall. However, ferric iron still present in the waste rocks and tailings may maintain AMD (Moses et al., 1987). Geochemical modelling at the TSF scale is underway and will give more arguments on the added value of an engineering cover over the TSF.

5.4. Climate change impact

Although the impact of climate change has not been simulated with the model, the water balance forecasts with the CMIP5 simulations are reassuring as to the possible evolution of recharge. An increase of the frequency and intensity of extreme events is expected for the end of the century. Analysis of climate variables under three RCP scenarios predicted a temperature rise of 0.5–5 °C until 2098 in the study area. Changes in annual rainfall have no significant pattern for all RCP scenarios. Regarding seasonal variation, summer should be drier with a rise of temperature and a decrease of rainfall as shown by Terray and Boé (2013). Regarding effective rainfall, few simulations show a significant trend (two out of 18) and for those two simulations, it is expected to decrease over the next 100 years. The Thornthwaite water balance method is not widely used to calculate effective rainfall in the future but it remains the simplest way to determine it (Aparecido et al., 2021). Nevertheless, this conclusion should be used with caution, as evapotranspiration could be impacted by changes in vegetation due to climate change (Laanaia et al., 2016). The major uncertainties in potential evapotranspiration come from the climate models (GCM and RCM) themselves (Lemaitre-Basset et al., 2021), the potential evapotranspiration formula being co-dependent on temperature. At the annual scale, if the effective rainfall were to decrease, the water volume to be treated would be lower and therefore the current environmental management of the site would remain valid in the future.

Extreme events due to climate change, both heatwaves and rain events, are expected to increase in France (Ouzeau et al., 2016; Trambly and Somot, 2018). The number of events will rise compared to the historical period (1975–2005). On the one hand, the analysis showed that extreme events in this area should be more frequent during the 21st century according to RCP2.6 and RCP8.5 scenarios. For RCP4.5, the number of events should almost double between 2006–2036 and 2068–2098. A study on six catchments near the Cévennes in southern France also showed that the frequency of extreme events could increase by 22 % at the end of the century compared to the period 1960–1990 (Trambly et al., 2012). Those results support the prediction that extreme events should be more frequent in the study basin, like in southern France. On the other hand, these extreme events should be more intense during the period 2068–2098 compared to the 2006–2036 period, according to the calculation of their return level using a maximum 3-day rainfall event per year, except for RCP8.5. This increase has also been predicted with an even greater increase of up to 22 % in extreme daily rainfall in the French Mediterranean (Ribes et al., 2019). This increase in rainfall during extreme events could impact the groundwater level below the TSF, allowing it to reach the tailings. Based on observation of short-period return events, the water table should not remain in contact with the tailings for more than five days. As seen in Section 5.1, extreme events could generate more AMD at the TSF outlet due to high pressure gradient in fine-textured materials such as the tailings. Extreme events may also have a different impact on the recharge depending on the season in which they occur (Manna et al., 2022). This impact is not taken into account by the Thornthwaite method, which is calculated on a monthly basis, independently of rainfall intensity. The extreme events occurring in summer are mainly due to storms with short and intense rainfall. This can lead to rapid flows into the storage which is flat and permeable. The low-intensity summer rainfall is mainly evapotranspired unlike winter rainfall which produces more infiltration and increases the water content in the unsaturated zone. Such impacts could not be analyzed with the available data.

6. Conclusion

The reclaimed Bertholène mine allows us to study the hydrogeological behavior of an anthropogenic site, to determine its potential modifications due to climate change and to provide guidance for sustainable environmental management in the future. The analysis developed in this study was supported by long-term field data. The installation of two new piezometers located in the tailings mining facility (TSF) and the implementation of a daily monitoring in several piezometers in the area provided new and accurate information at the site scale. The groundwater level analysis showed that the facility is in an unsaturated condition throughout the year including during recorded extreme rainfall events. Correlations between rainfall and discharges confirmed the fast response of the catchment. At the TSF outlet, the water collected at the control basin consists of at least 70 % of water from the gneiss aquifer and up to 30 % from vertical seepage through the unsaturated tailings during high-flow periods.

A three-dimensional simplified groundwater flow model was developed to understand the steady-state functioning of the mining catchment based on the analysis of monitored data, and to identify the groundwater flow paths. The model's input is the recharge calculated from the water balance at the catchment scale (Q Venturi). The model was used to test the impacts of a reclamation scenario. A cover over the TSF could lower groundwater levels by 1 m at the site scale and decrease the discharge at the BC by 20 %. The cover would slightly reduce the AMD at the outlet of the TSF, with only water coming from the gneiss aquifer reaching the control basin. Since AMD is generated elsewhere in the mine site, the treatment station should continue to operate with or without TSF coverage. The geochemical model should provide new information on how long AMD is expected to last in the near future at the TSF scale. This will make an informed decision on the added value of the TSF cover.

Climate change is expected to have little effect on the hydrological functioning of the catchment. With only two out of the 18 evaluated models giving a significant trend of decreasing effective rainfall, the recharge might slightly decrease at the site, leading to lower water levels and discharges compared to the current situation. Climate change, on the other hand, will have an impact on extreme events. They should be more frequent and more intense than during the historical period in the catchment area. At the end of the century and compared to the period 2006–2036, events should not be more frequent except for the RCP4.5 scenario. For the RCP2.6 and RCP4.5 scenarios, the intensity of an event for a given return period would increase by 4 % compared to a 4 % decrease for the RCP8.5 scenario. This means that the water table could reach the tailings during some extreme events but only for a few days. The impact of such an event in terms of geochemical reaction should be evaluated. Overall, the climate change study shows that the current hydrological functioning of the site remains valid in the future.

The methodology developed here is not site-specific and is applicable to other sites with some adaptations regarding the site's characteristics and modeling expectations. Daily frequency monitoring appears essential to understand the functioning of the catchment as it gives information regarding the water table reactivity, its interaction with the tailings especially during extreme events and the discharge reaction to rainfall. The combination of data analysis with groundwater modeling is very useful for testing and (in) validating different hypotheses about groundwater flow paths and water sources. It is also useful for testing reclamation scenario. However steady-state modelling does not simulate the fate of the site under climate change and extreme events. In our case, this simple modeling methodology only provides the average state of the hydrogeological system, determines the sub-catchments and identifies the origin of the water at BC, all based on a detailed data analysis. The use of climate change projections is necessary to evaluate the impact of future rainfall and temperature variations on the effective rainfall. It may be more appropriate to run the model with climate change data as input if changes in recharge were significant, which is not the case here. Similarly for extreme events, a transient model would allow to simulate the response of the catchment in wet and dry periods and to see the resulting variations of groundwater levels as well as discharges. Pending the results of the geochemical study and from a hydrogeological point of view, this study validates the current management for this former mine. The geochemical study under development will focus on 1D and 2D modeling of the TSF in unsaturated conditions in order to quantify the duration of AMD generation. [Beaucaire \(2021\)](#) worked with a model in saturated conditions and with a lack of data regarding the petro-physical and mineralogical properties of the stored materials. These two limits justify that the estimate of the end of AMD generation, already proposed, must be taken with caution, especially since the amount of pyrite remaining in the storage is not known. Through the hydrogeological model and data monitoring, the flow conditions in the TSF and the origin and discharges evolution at the outlet of the TSF were clarified. Thus, the geochemical model will be better constrained and could be run in transient conditions given the influence of extreme events in the unsaturated zone.

Funding

This research was funded by ORANO Group Environmental R&D (France) and received no external funding.

CRedit authorship contribution statement

Pierre L'Hermite: Conceptualization, Methodology, Investigation, Software, Validation, Formal analysis, Visualization, Writing – review & editing. **Valérie Plagnes:** Conceptualization, Methodology, Validation, Visualization, Supervision, Writing – review & editing. **Anne Jost:** Conceptualization, Methodology, Validation, Visualization, Supervision, Writing – review & editing. **Guillaume Kern:** Investigation, Resources, Review. **Benoît Reilé:** Investigation, Resources, Review. **Camille Chautard:** Conceptualization, Resources, Review. **Michael Descostes:** Conceptualization, Methodology, Investigation, Validation, Supervision, Review.

Authors statement

All authors have read and approved the final version of this manuscript and do not have any conflicts of interest associated with this publication.

Declaration of Competing Interest

The authors declare that they have no known competing financial interests or personal relationships that could have appeared to influence the work reported in this paper. The authors thank Isabelle Blanc-Potard, Mathieu Corbrejaud and Elodie Tétard from ORANO Mining Après Mines France for their availability and for providing historical data. Thanks are also due to Ludovic Oudin and Thibault Lemaitre-Basset from Sorbonne Université for their recommendations and comments about climate change impact.

Data Availability

The authors do not have permission to share data.

Appendix A. Supporting information

Supplementary data associated with this article can be found in the online version at [doi:10.1016/j.ejrh.2022.101221](https://doi.org/10.1016/j.ejrh.2022.101221).

References

- IAEA, OECD, 2002. Environmental Remediation of Uranium Production Facilities, Nuclear Development. OECD Publishing. <https://doi.org/10.1787/9789264194809-en>.
- IPCC, 2014. In: Pachauri, R.K., Meyer, L.A. (Eds.), *Climate Change 2014: Synthesis Report. Contribution of Working Groups I, II and III to the Fifth Assessment Report of the Intergovernmental Panel on Climate Change [Core Writing Team. IPCC, Geneva, Switzerland, p. 151.*
- American Society of Civil Engineers, 1969. Design and Construction of Sanitary and Storm Sewers. American Society of Civil Engineers and the Water Pollution Control Federation, New York.
- Akcil, A., Koldas, S., 2006. Acid Mine Drainage (AMD): causes, treatment and case studies. *J. Clean. Prod., Improving Environmental, Economic and Ethical Performance in the Mining Industry. Part 2. Life cycle and process analysis and technical issues* 14, 1139–1145. <https://doi.org/10.1016/j.jclepro.2004.09.006>.
- An, N.N., Nhut, H.S., Phuong, T.A., Huy, V.Q., Hanh, N.C., Thao, G.T.P., Trinh, P.T., Hoa, P.V., Binh, N.A., 2022. Groundwater simulation in Dak Lak province based on MODFLOW model and climate change scenarios. *Front. Eng. Built Environ.* 2, 55–67. <https://doi.org/10.1108/FEBE-11-2021-0055>.
- Aparedo, L.E., Lorençone, P., Lorençone, J., Meneses, K., Moraes, J., 2021. Climate changes and their influences in water balance of Pantanal biome. *Theor. Appl. Clim.* 143. <https://doi.org/10.1007/s00704-020-03445-4>.
- Aquaveo, 2017. Groundwater Modeling System [WWW Document]. URL (<https://www.aquaveo.com/software/gms-groundwater-modeling-system-introduction>) (accessed 2.10.21).
- Aubertin, M., Bussièrre, B., Pabst, T., James, M., Mbonimpa, M., 2016. Review of the reclamation techniques for acid-generating mine wastes upon closure of disposal sites. *Geo-Chicago 2016*. Presented at the Geo-Chicago 2016. American Society of Civil Engineers, Chicago, Illinois, pp. 343–358. <https://doi.org/10.1061/9780784480137.034>.
- Aubertin, M., Fala, O., Bussièrre, B., Martin, V., Campos, D., Gamache-Rochette, A., Chouteau, M., Chapuis, R., 2002. Analyse des écoulements de l'eau en conditions non saturées dans les haldes à stériles. *Comptes-rendus du Symposium 2002 sur l'Environnement et les Mines Rouyn-Noranda Québec Canada*.
- IPCC, 2021. *Climate Change 2021: The Physical Science Basis. (Contribution of Working Group I to the Sixth Assessment Report of the Intergovernmental Panel on Climate Change)*. Cambridge University Press.
- Ballini, M., Chautard, C., Nos, J., Phrommavanh, V., Beaucaire, C., Besançon, C., Boizard, A., Cathelineau, M., Peiffert, C., Vercouter, T., Vors, E., Descostes, M., 2020. A multi-scalar study of the long-term reactivity of uranium mill tailings from Bellezane site (France). *J. Environ. Radioact.* 218, 106223 <https://doi.org/10.1016/j.jenvrad.2020.106223>.
- Barnett, B., Townley, L., Post, V., Evans, R., Hunt, R., Peeters, L., Richardson, S., Werner, A., Knapton, A., Boronkay, A., 2012. Australian Groundwater Modelling Guidelines.
- Beaucaire, C., 2021. Modélisation géochimique du drainage acide minier au sein du stockage de résidus de Bertholène (Technical Report No. IDF-DT-009383). Orano Mining.
- Bell, F.G., Bullock, S.E.T., Haelbich, T.F.J., Lindsay, P., 2001. Environmental impacts associated with an abandoned mine in the Witbank Coalfield, South Africa. *Int. J. Coal Geol.* 45, 195–216.
- Besançon, C., Chautard, C., Beaucaire, C., Savoye, S., Sardini, P., Gérard, M., Descostes, M., 2020. The role of barite in the post-mining stabilization of radium-226: a modeling contribution for sequential extractions. *Minerals* 10, 497. <https://doi.org/10.3390/min10060497>.
- Blowes, D.W., Ptacek, C.J., Jambor, J.L., Weisener, C.G., Paktunc, D., Gould, W.D., Johnson, D.B., 2014. 11.5 the geochemistry of acid mine drainage. *Treatise Geochem.* 131–190. <https://doi.org/10.1016/b978-0-08-095975-7.00905-0>.
- BRGM, 1997. Les résidus miniers français: typologie et principaux impacts environnementaux potentiels (Rapport No. R-39503). BRGM.
- Brigode, P., Génot, B., Lobligeois, F., Delaigue, O., 2020. Summary sheets of watershed-scale hydroclimatic observed data for France. <https://doi.org/10.15454/UV01P1>.
- Bussièrre, B., 2010. Acid mine drainage from abandoned mine sites: problematic and reclamation approaches. In: Chen, Y., Zhan, L., Tang, X. (Eds.), *Advances in Environmental Geotechnics*. Springer Berlin Heidelberg, Berlin, Heidelberg, pp. 111–125. https://doi.org/10.1007/978-3-642-04460-1_6.
- Chautard, C., Beaucaire, C., Gérard, M., Roy, R., Savoye, S., Descostes, M., 2020. Geochemical characterization of uranium mill tailings (Bois Noirs Limouzat, France) highlighting the U and 226Ra retention. *J. Environ. Radioact.* 218, 106251 <https://doi.org/10.1016/j.jenvrad.2020.106251>.
- Chautard, C., Beaucaire, C., Gérard, M., Phrommavanh, V., Nos, J., Galoisy, L., Calas, G., Roy, R., Descostes, M., 2017. Geochemical Characterization of U Tailings (Bois Noirs Limouzat, France). *Procedia Earth Planet. Sci.* 17, 308–311. <https://doi.org/10.1016/j.proeps.2016.12.067>.
- Collet, L., Beevers, L., Prudhomme, C., 2017. Assessing the impact of climate change and extreme value uncertainty to extreme flows across Great Britain. *Water* 9, 103. <https://doi.org/10.3390/w9020103>.
- Déjeant, A., Bourva, L., Sia, R., Galoisy, L., Calas, G., Phrommavanh, V., Descostes, M., 2014. Field analyses of 238U and 226Ra in two uranium mill tailings piles from Niger using portable HPGe detector. *J. Environ. Radioact.* 137, 105–112. <https://doi.org/10.1016/j.jenvrad.2014.06.012>.

- Déjeant, A., Galois, L., Roy, R., Calas, G., Boekhout, F., Phrommavanh, V., Descostes, M., 2016. Evolution of uranium distribution and speciation in mill tailings, COMINAK Mine, Niger. *Sci. Total Environ.* 545–546, 340–352. <https://doi.org/10.1016/j.scitotenv.2015.12.027>.
- Déqué, M., 2007. Frequency of precipitation and temperature extremes over France in an anthropogenic scenario: Model results and statistical correction according to observed values. *Glob. Planet. Change Extrem. Clim. Events* 57, 16–26. <https://doi.org/10.1016/j.gloplacha.2006.11.030>.
- Descostes, M., Vitorge, P., Beaucaire, C., 2004. Pyrite dissolution in acidic media.
- Dewandel, B., Lachassagne, P., Wyns, R., Maréchal, J.C., Krishnamurthy, N.S., 2006. A generalized 3-D geological and hydrogeological conceptual model of granite aquifers controlled by single or multiphase weathering. *J. Hydrol.* 330, 260–284. <https://doi.org/10.1016/j.jhydrol.2006.03.026>.
- Didovets, I., Krysanova, V., Hattermann, F.F., del Rocio Rivas López, M., Snizhko, S., Müller Schmied, H., 2020. Climate change impact on water availability of main river basins in Ukraine. *J. Hydrol. Reg. Stud.* 32, 100761 <https://doi.org/10.1016/j.ejrh.2020.100761>.
- Ethier, M.-P., Bussiére, B., Broda, S., Aubertin, M., 2018. Three-dimensional hydrogeological modeling to assess the elevated-water-table technique for controlling acid generation from an abandoned tailings site in Quebec, Canada. *Hydrogeol. J.* 26, 1201–1219. <https://doi.org/10.1007/s10040-017-1713-y>.
- Fiorillo, F., Doglioni, A., 2010. The relation between karst spring discharge and rainfall by cross-correlation analysis (Campania, southern Italy). *Hydrogeol. J.* 18, 1881–1895. <https://doi.org/10.1007/s10040-010-0666-1>.
- Fisher, R.A., Tippett, L.H.C., 1928. Limiting forms of the frequency distribution of the largest or smallest member of a sample. *Proc. Camb. Philos. Soc.* 24, 180–190.
- Galván, L., Olfas, M., Cánovas, C.R., Sarmiento, A.M., Nieto, J.M., 2016. Hydrological modeling of a watershed affected by acid mine drainage (Odiel River, SW Spain). Assessment of the pollutant contributing areas. *J. Hydrol.* 540, 196–206. <https://doi.org/10.1016/j.jhydrol.2016.06.005>.
- Gaur, Ayushi, Gaur, Abhishek, Simonovic, S.P., 2018. Future changes in flood hazards across Canada under a Changing Climate. *Water* 10, 1441. <https://doi.org/10.3390/w10101441>.
- Géostock, 1993. Reconnaissance hydrogéologique de la veine et du site (No. GK/BER-93/051; BVH/EAM/IT).
- González-Quiros, A., Fernández-Álvarez, J.P., 2019. Conceptualization and finite element groundwater flow modeling of a flooded underground mine reservoir in the Asturian Coal Basin, Spain. *J. Hydrol.* 578, 124036 <https://doi.org/10.1016/j.jhydrol.2019.124036>.
- Hamed, K.H., Ramachandra Rao, A., 1998. A modified Mann-Kendall trend test for autocorrelated data. *J. Hydrol.* 204, 182–196. [https://doi.org/10.1016/S0022-1694\(97\)00125-X](https://doi.org/10.1016/S0022-1694(97)00125-X).
- Harbaugh, A.W., 2005. MODFLOW-2005: the U.S. geological survey modular ground-water model—the ground-water flow process. *US Geol. Surv.* <https://doi.org/10.3133/tm6a16>.
- Hatje, V., Pedreira, R.M.A., de Rezende, C.E., Schettini, C.A.F., de Souza, G.C., Marin, D.C., Hackspacher, P.C., 2017. The environmental impacts of one of the largest tailing dam failures worldwide. *Sci. Rep.* 7, 10706. <https://doi.org/10.1038/s41598-017-11143-x>.
- Henriksen, H.J., Jakobsen, A., Pasten-Zapata, E., Tordborg, L., Sonnenborg, T.O., 2021. Assessing the impacts of climate change on hydrological regimes and fish EQR in two Danish catchments. *J. Hydrol. Reg. Stud.* 34, 100798 <https://doi.org/10.1016/j.ejrh.2021.100798>.
- Herr, J., Chen, C., Goldstein, R., Herd, R., Brown, J., 2007. Modeling acid mine drainage on a watershed scale for TMDL calculations. *JAWRA J. Am. Water Resour. Assoc.* 39, 289–300. <https://doi.org/10.1111/j.1752-1688.2003.tb04384.x>.
- Hotton, G., Bussiére, B., Pabst, T., Bresson, E., Roy, P., 2020. Influence of climate change on the ability of a cover with capillary barrier effects to control acid generation. *Hydrogeol. J.* 28, 763–779. <https://doi.org/10.1007/s10040-019-02084-y>.
- Kalisman, D., Yakirevich, A., Sorek, S., Kamai, T., 2022. Enhancing solute transport by pressure-wave driven flow in unsaturated porous media. *J. Hydrol.* 612, 128196 <https://doi.org/10.1016/j.jhydrol.2022.128196>.
- Kendall, M.G., 1975. Rank Correlation methods.
- Khoern, K., Sakaguchi, A., Tomiyama, S., Igarashi, T., 2019. Long-term acid generation and heavy metal leaching from the tailings of Shimokawa mine, Hokkaido, Japan: Column study under natural condition. *J. Geochem. Explor.* 201, 1–12. <https://doi.org/10.1016/j.gexplo.2019.03.003>.
- Laanaia, N., Carrer, D., Calvet, J.-C., Pagé, C., 2016. How will climate change affect the vegetation cycle over France? A generic modeling approach. *Clim. Risk Manag.* 13, 31–42. <https://doi.org/10.1016/j.crm.2016.06.001>.
- Labonté-Raymond, P.-L., Pabst, T., Bussiére, B., Bresson, E., 2020. Impact of climate change on extreme rainfall events and surface water management at mine waste storage facilities. *J. Hydrol.* 590, 125383 <https://doi.org/10.1016/j.jhydrol.2020.125383>.
- Lahrouch, F., Guo, N., Hunault, M.O.J.Y., Solari, P.L., Descostes, M., Gerard, M., 2021. Uranium retention on iron oxyhydroxides in post-mining environmental conditions. *Chemosphere* 264, 128473. <https://doi.org/10.1016/j.chemosphere.2020.128473>.
- Larocque, M., Mangin, A., Razack, M., Banton, O., 1998. Contribution of correlation and spectral analyses to the regional study of a large karst aquifer (Charente, France). *J. Hydrol.* 205, 217–231. [https://doi.org/10.1016/S0022-1694\(97\)00155-8](https://doi.org/10.1016/S0022-1694(97)00155-8).
- Ledoux, E., Schmitt, J.-M., Combes, P., 1993. Etude hydrologique et hydrogéochimique du site minier de Bertholène (No. LHM/RD/93/93). Ecole des mines de Paris.
- Lemaître-Basset, T., Oudin, L., Thirel, G., Collet, L., 2021. Uncertainty on evapotranspiration formulation and its hydrological implication under climate change over France (other). *Pico*. <https://doi.org/10.5194/egusphere-egu21-9946>.
- Lersow, M., 2010. Safe closure of uranium mill tailings ponds - on basis of long-term stability-proofs linked with an extensive environmental monitoring. <https://doi.org/10.13140/RG.2.1.4805.7364>.
- Lestini, L., Beaucaire, C., Vercouter, T., Ballini, M., Descostes, M., 2019. Role of Trace Elements in the 226-Radium Incorporation in Sulfate Minerals (Gypsum and Celestite). *ACS Earth Space Chem.* 3, 295–304. <https://doi.org/10.1021/acsearthspacechem.8b00150>.
- Lieber, E., Demers, I., Pabst, T., Bresson, E., 2022. Simulating the effect of climate change on performance of a monolayer cover combined with an elevated water table placed on acid-generating mine tailings. *Can. Geotech. J.* 59, 558–568. <https://doi.org/10.1139/cgj-2020-0622>.
- Mamo, S., Birhanu, B., Ayenew, T., Taye, G., 2021. Three-dimensional groundwater flow modeling to assess the impacts of the increase in abstraction and recharge reduction on the groundwater, groundwater availability and groundwater-surface waters interaction: a case of the rib catchment in the Lake Tana sub-basin of the Upper Blue Nile River, Ethiopia. *J. Hydrol. Reg. Stud.* 35, 100831 <https://doi.org/10.1016/j.ejrh.2021.100831>.
- Mann, H.B., 1945. NonParametric tests against trend Vol. 13.
- Manna, F., Kennel, J., Parker, B.L., 2022. Understanding mechanisms of recharge through fractured sandstone using high-frequency water-level-response data. *Hydrogeol. J.* 30, 1599–1618. <https://doi.org/10.1007/s10040-022-02515-3>.
- Maréchal, J.-C., Wyns, R., Lachassagne, P., Subrahmanyam, K., 2004. Vertical anisotropy of hydraulic conductivity in the fissured layer of hard-rock aquifers due to the geological structure of weathering profiles. *J. Geol. Soc. India* 63, 545–550.
- Mengistu, H., Tessema, A., Abiye, T., Demlie, M., Lin, H., 2015. Numerical modeling and environmental isotope methods in integrated mine-water management: a case study from the Witwatersrand basin, South Africa. *Hydrogeol. J.* 23, 533–550. <https://doi.org/10.1007/s10040-014-1216-z>.
- Mengistu, H.A., Demlie, M.B., Abiye, T.A., Xu, Y., Kanyerere, T., 2019. Conceptual hydrogeological and numerical groundwater flow modelling around the Moab Khutsong deep gold mine, South Africa. *Groundw. Sustain. Dev.* 9, 100266 <https://doi.org/10.1016/j.gsd.2019.100266>.
- Orano Mining, 2021. Dossier d'information - Après-Mines France. Orano.
- Moses, C.O., Kirk Nordstrom, D., Herman, J.S., Mills, A.L., 1987. Aqueous pyrite oxidation by dissolved oxygen and by ferric iron. *Geochim. Cosmochim. Acta* 51, 1561–1571. [https://doi.org/10.1016/0016-7037\(87\)90337-1](https://doi.org/10.1016/0016-7037(87)90337-1).
- Niekerk, H.J.V., Viljoen, M.J., 2005. Causes and consequences of the Merriespruit and other tailings-dam failures. *Land Degrad. Dev.* 16, 201–212. <https://doi.org/10.1002/ldr.681>.
- Oudin, L., Hervieu, F., Michel, C., Perrin, C., Andréassian, V., Anctil, F., Loumagne, C., 2005. Which potential evapotranspiration input for a lumped rainfall–runoff model? *J. Hydrol.* 303, 290–306. <https://doi.org/10.1016/j.jhydrol.2004.08.026>.
- Ouzeau, G., Soubeyroux, J.-M., Schneider, M., Vautard, R., Planton, S., 2016. Heat waves analysis over France in present and future climate: application of a new method on the EURO-CORDEX ensemble. *Clim. Serv.* 4, 1–12. <https://doi.org/10.1016/j.cliser.2016.09.002>.
- Petpongpan, C., Ekkawatpanit, C., Visessri, S., Kositgittiwong, D., 2021. Projection of hydro-climatic extreme events under climate change in Yom and Nan River Basins, Thailand. *Water* 13, 665. <https://doi.org/10.3390/w13050665>.

- Rapantova, N., Grmela, A., Vojtek, D., Halir, J., Michalek, B., 2007. Ground water flow modelling applications in mining hydrogeology. *Mine Water Environ.* 26, 264–270. <https://doi.org/10.1007/s10230-007-0017-1>.
- Ribes, A., Thao, S., Vautard, R., Dubuisson, B., Somot, S., Colin, J., Planton, S., Soubeyroux, J.-M., 2019. Observed increase in extreme daily rainfall in the French Mediterranean. *Clim. Dyn.* 52, 1095–1114. <https://doi.org/10.1007/s00382-018-4179-2>.
- Sahu, P., López, D.L., Stoertz, M.W., 2009. Using time series analysis of coal mine hydrographs to estimate mine storage, retention time, and mine-pool interconnection. *Mine Water Environ.* 28, 194–205. <https://doi.org/10.1007/s10230-009-0076-6>.
- Santos, E.B., Lucio, P.S., Santos e Silva, C.M., 2016. Estimating return periods for daily precipitation extreme events over the Brazilian Amazon. *Theor. Appl. Climatol.* 126, 585–595. <https://doi.org/10.1007/s00704-015-1605-9>.
- Schmitt, J.M., Lions, J., Ledoux, E., 2002. Réévaluation de l'évolution hydrogéologique et hydrochimique du site de Bertholène (Aveyron): modélisation prédictive intégrée de l'ensemble du site minier (No. LHM/RD/02/23). Ecole des mines de Paris.
- Schmitt, J.-M., Tardy, Y., 1986. Albittisation triasique, hydrothermalisme jurassique et altération supergène récente: métallogénie des gisements uranifères du Rouergue. *Strasbourg 1*.
- Seigneur, N., De Windt, L., Déjeant, A., Lagneau, V., Descostes, M., 2021. Long-term evolution of uranium mobility within sulfated mill tailings in arid regions: a reactive transport study. *Minerals* 11, 1201. <https://doi.org/10.3390/min11111201>.
- Sen, P.K., 1968. Estimates of the regression coefficient based on Kendall's Tau. *J. Am. Stat. Assoc.* 63, 1379–1389. <https://doi.org/10.2307/2285891>.
- Soubeyroux, J.-M., Bernus, S., Corre, L., Drouin, A., Dubuisson, B., Etchevers, P., Guget, V., Josse, P., Kerdoncuff, M., Samacoits, R., Tocquer, F., 2020. Les nouvelles projections climatiques de référence DRIAS 2020 pour la métropole. Météo France.
- Surinaidu, L., Rao, V.V.S.G., Rao, N.S., Srinu, S., 2014. Hydrogeological and groundwater modeling studies to estimate the groundwater inflows into the coal Mines at different mine development stages using MODFLOW, Andhra Pradesh, India. *Water Resour. Ind.* 7–8, 49–65. <https://doi.org/10.1016/j.wri.2014.10.002>.
- Tabelin, C.B., Igarashi, T., Villacorte-Tabelin, M., Park, I., Opiso, E.M., Ito, M., Hiroyoshi, N., 2018. Arsenic, selenium, boron, lead, cadmium, copper, and zinc in naturally contaminated rocks: a review of their sources, modes of enrichment, mechanisms of release, and mitigation strategies. *Sci. Total Environ.* 645, 1522–1553. <https://doi.org/10.1016/j.scitotenv.2018.07.103>.
- Terray, L., Boé, J., 2013. Quantifying 21st-century France climate change and related uncertainties. *Comptes Rendus Geosci.* 345, 136–149. <https://doi.org/10.1016/j.crte.2013.02.003>.
- Thornthwaite, C.W., 1948. An approach toward a rational classification of climate. *Geogr. Rev.* 38, 55. <https://doi.org/10.2307/210739>.
- Tirogo, J., Jost, A., Biaou, A., Valdes-Lao, D., Koussoubé, Y., Ribstein, P., 2016. Climate variability and groundwater response: a case study in Burkina Faso (West Africa). *Water* 8, 171. <https://doi.org/10.3390/w8050171>.
- Tomiyaama, S., Igarashi, T., Tabelin, C.B., Tangviroon, P., Ii, H., 2020. Modeling of the groundwater flow system in excavated areas of an abandoned mine. *J. Contam. Hydrol.* 230, 103617. <https://doi.org/10.1016/j.jconhyd.2020.103617>.
- Tramblay, Y., Somot, S., 2018. Future evolution of extreme precipitation in the Mediterranean. *Clim. Change* 151, 289–302. <https://doi.org/10.1007/s10584-018-2300-5>.
- Tramblay, Y., Neppel, L., Carreau, J., Sanchez-Gomez, E., 2012. Extreme value modelling of daily areal rainfall over Mediterranean catchments in a changing climate: daily areal rainfall over mediterranean catchments. *Hydrol. Process.* 26, 3934–3944. <https://doi.org/10.1002/hyp.8417>.
- Triganon, A., 2013. Modélisation hydrogéologique et géochimique du drainage acide minier du site de Bertholène – APS d'aménagement pour limiter les rejets du site (Prestation No. RBENSE0305- 03). BURGEAP.
- Verfaillie, D., Déqué, M., Morin, S., Lafayesse, M., 2017. The method ADAMONT v1.0 for statistical adjustment of climate projections applicable to energy balance land surface models. *Geosci. Model Dev.* 10, 4257–4283. <https://doi.org/10.5194/gmd-10-4257-2017>.
- WMA, 2020. World Uranium Mining - World Nuclear Association [WWW Document]. URL (<https://www.world-nuclear.org/information-library/nuclear-fuel-cycle/mining-of-uranium/world-uranium-mining-production.aspx>) (accessed 1.29.21).
- Wolkersdorfer, C., Nordstrom, D.K., Beckie, R.D., Cicerone, D.S., Elliot, T., Edraki, M., Valente, T., França, S.C.A., Kumar, P., Lucero, R.A.O., Soler i Gil, A., 2020. Guidance for the integrated use of hydrological, geochemical, and isotopic tools in mining operations. *Mine Water Environ.* 39, 204–228. <https://doi.org/10.1007/s10230-020-00666-x>.